

Phenomenology of a little Higgs pseudoaxion

Kingman Cheung,^{1,2,3,*} Shi-Ping He,^{4,†} Ying-nan Mao,^{1,5,‡} Po-Yan Tseng,^{6,§} and Chen Zhang^{1,||}

¹*Physics Division, National Center for Theoretical Sciences, Hsinchu, Taiwan 300*

²*Department of Physics, National Tsing Hua University, Hsinchu 300, Taiwan*

³*Division of Quantum Phases and Devices, School of Physics, Konkuk University, Seoul 143-701, Republic of Korea*

⁴*Institute of Theoretical Physics & State Key Laboratory of Nuclear Physics and Technology, Peking University, Beijing 100871, China*

⁵*Center for Future High Energy Physics & Theoretical Physics Division, Institute of High Energy Physics, Chinese Academy of Sciences, Beijing 100049, China*

⁶*Kavli IPMU (WPI), UTIAS, The University of Tokyo, Kashiwa, Chiba 277-8583, Japan*



(Received 19 September 2018; published 29 October 2018)

In models where the Higgs is realized as a pseudo-Nambu-Goldstone boson (pNGB) of some global symmetry breaking, there are often remaining pNGBs of some $U(1)$ groups (called “pseudoaxions”) which could lead to smoking-gun signatures of such scenarios and provide important clues on the electroweak symmetry breaking mechanism. As a concrete example, we investigate the phenomenology of the pseudoaxion in the anomaly-free simplest little Higgs (SLH) model. After clarifying a subtle issue related to the effect of symmetric vector-scalar-scalar vertices [e.g., $Z_\mu(H\partial^\mu\eta + \eta\partial^\mu H)$], we show that for a natural region in the parameter space, the SLH pseudoaxion is top-philic, decaying almost exclusively to a pair of top quarks. The direct and indirect (i.e., via heavy particle decay) production of such a pseudoaxion at the 14 TeV (HL-)LHC turn out to suffer from either large backgrounds or small rates, making its detection quite challenging. A pp collider with higher energy and luminosity, such as the 27 TeV HE-LHC, or even the 100 TeV FCC-hh or SppC, is therefore motivated to capture the trace of such a pNGB.

DOI: [10.1103/PhysRevD.98.075023](https://doi.org/10.1103/PhysRevD.98.075023)

I. INTRODUCTION

Despite the great success of the Standard Model (SM), marked by the discovery of the 125 GeV Higgs-like boson [1,2] and the ongoing measurements of its properties, how the SM is embedded into a larger theory still remains a mystery. Since the Higgs boson mass parameter is in general not protected under radiative correction, a naive embedding would signal a high sensitivity of infrared (IR) parameters (the electroweak scale and the Higgs boson mass) to ultraviolet (UV) parameters (i.e., physical parameters defined at a high scale). Although this fine-tuned situation is logically possible, or might be explained to some extent by anthropic reasoning [3,4], it is nevertheless

natural to conjecture the existence of some systematic mechanism which protects the Higgs boson mass parameter from severe radiative instability. A well-known example of such a systematic mechanism is supersymmetry, which has the merit of being weakly coupled and thus offers better calculability compared to scenarios based on strong dynamics. However, supersymmetry requires the introduction of a large number of new degrees of freedom (d.o.f.), and a large number of new parameters associated with them, making the model quite cumbersome. None of the new d.o.f. have been observed. It is therefore well motivated to consider alternative but simpler mechanisms with weakly coupled dynamics in their range of validity.

One candidate of such an alternative is the little Higgs mechanism [5–8],¹ in which the Higgs boson is a Goldstone boson of some spontaneous global symmetry breaking. The global symmetry is also explicitly broken in a collective manner² such that the Higgs boson acquires a

¹We refer the reader to Refs. [9,10] for reviews of little Higgs models and Refs. [11–14] for some recent phenomenological analyses of little Higgs models.

²More specifically, the global symmetry is completely (explicitly) broken by a collection of spurions but not by any single spurion [8].

*cheung@phys.nthu.edu.tw

†sphe@pku.edu.cn

‡ynmao@cts.nthu.edu.tw

§poyen.tseng@ipmu.jp

||czhang@cts.nthu.edu.tw

Published by the American Physical Society under the terms of the *Creative Commons Attribution 4.0 International license*. Further distribution of this work must maintain attribution to the author(s) and the published article’s title, journal citation, and DOI. Funded by SCOAP³.

mass and at the same time the model is radiatively more stable. A very simple implementation of this collective symmetry breaking (CSB) idea is the simplest little Higgs (SLH) model [15,16], in which the electroweak gauge group is enlarged to $SU(3)_L \times U(1)_X$, and two scalar triplets are introduced to realize the global symmetry-breaking pattern

$$\begin{aligned} & [SU(3)_1 \times U(1)_1] \times [SU(3)_2 \times U(1)_2] \\ & \rightarrow [SU(2)_1 \times U(1)_1] \times [SU(2)_2 \times U(1)_2]. \end{aligned} \quad (1)$$

The global symmetry is also explicitly broken by gauge and Yukawa interactions, but in a collective manner to improve the radiative stability of the scalar sector. The particle content is quite economical. In particular, in the low-energy scalar sector there exists only two physical d.o.f., one of which (denoted H) could be identified with the 125 GeV Higgs-like particle, while the other is a CP -odd scalar η which is referred to as a pseudoaxion in the literature [17,18].

In the SLH, the pseudoaxion η is closely related to the electroweak symmetry breaking (EWSB) and therefore studying its phenomenology is well motivated. According to the hidden mass relation derived in Ref. [19], the η mass m_η is anticorrelated with the top partner mass m_T , which is in turn related to the degree of fine-tuning in the model. The hidden mass relation is derived within an approach consistent with the continuum effective field theory (CEFT) and does not rely on the assumption on the contribution from the physics at the cutoff. Although the phenomenology of the η particle has been studied in quite a few papers (e.g., Refs. [14,17,18,20,21]), their treatment was not based on the hidden mass relation, and also most of the papers were written before the 125 GeV boson was discovered. It is thus timely to revisit the status of η phenomenology in light of the discovery of the 125 GeV boson, taking into account the properly derived hidden mass relation and focusing on the parameter space favored by naturalness considerations.

There is another important reason that warrants a reanalysis of the η phenomenology. The SLH is usually written as a gauged nonlinear sigma model, in which the EWSB can be parametrized through vacuum misalignment. However, the vacuum misalignment also leads to the fact that, in the usual parametrization of the two scalar triplets, there exist scalar kinetic terms that are not canonically normalized, and vector-scalar two-point transitions that are “unexpected” [22]. A further field rotation, including an appropriate gauge-fixing procedure, is thus required to properly diagonalize the vector-scalar sector of the SLH model. This subtlety was overlooked in all related papers before Ref. [22], and if one carries out a proper diagonalization of the bosonic sector of the SLH, some of the η -related couplings will turn out to be different from what has been obtained in previous literature. This is the case for both the $ZH\eta$ coupling and the coupling of η to a pair of SM fermions. The occurrence of the mass eigenstate

antisymmetric $ZH\eta$ vertex [i.e., $Z_\mu(H\partial^\mu\eta - \eta\partial^\mu H)$] is postponed to $\mathcal{O}(\xi^3)$ [where $\xi \equiv \frac{v}{f}$, $v \approx 246$ GeV and f is the global symmetry-breaking scale of Eq. (1)], and the couplings of η to a pair of SM charged leptons, and to $b\bar{b}$, $c\bar{c}$, $u\bar{u}$ are found to vanish to all orders in ξ . This leads to significant changes in the η phenomenology, which will be studied in detail in this work.

When one tries to derive the η -related Lagrangian in the SLH, symmetric vector-scalar-scalar (VSS) vertices, e.g., $Z_\mu(H\partial^\mu\eta + \eta\partial^\mu H)$ naturally appear, which is a feature that is often present in models based on a nonlinearly realized scalar sector. The effects of such symmetric VSS vertices contain some subtleties which, to our knowledge, have not been discussed before in the literature. Therefore, we devote one section to the analysis of symmetric VSS vertices, which could also be helpful to clarify similar situations in other nonlinearly realized models.

In this work we do not aim to give a complete characterization of the η phenomenology, which could be very complicated in certain corners of parameter space. Instead, we focus our attention on the parameter space favored by naturalness considerations. More specifically, we will consider an η mass in the region $2m_t \lesssim m_\eta \lesssim 1$ TeV, which is favored by naturalness. We then calculate the η decay and production at future high-energy hadron colliders in various channels. It turns out that at the 14 TeV (HL)-LHC the detection of η is quite challenging due to various suppression mechanisms. A pp collider with higher energy and luminosity, such as the 27 TeV HE-LHC, or even the 100 TeV FCC-hh or SppC, is therefore motivated to capture the trace of such a pNGB.

The paper is organized as follows. In Sec. II we review the basic ingredients of the SLH, including the crucial hidden mass relation obtained from a CEFT analysis, and present the mass eigenstate Lagrangian relevant for phenomenological studies. In Sec. III we clarify the effect of symmetric VSS vertices. Then, in Sec. IV we derive important constraints from electroweak precision observables relevant for the pseudoaxion phenomenology. Section V is dedicated to the study of η decay and production at hadron colliders. In Sec. VI we present the discussion and conclusions.

II. THE SIMPLEST LITTLE HIGGS

A. Overview of the simplest little Higgs

In the SLH, the electroweak gauge group is enlarged to $SU(3)_L \times U(1)_X$. Two scalar triplets Φ_1, Φ_2 are introduced to realize the spontaneous global symmetry breaking pattern in Eq. (1). They are parametrized as

$$\Phi_1 = \exp\left(\frac{i\Theta'}{f}\right) \exp\left(\frac{it_\beta\Theta}{f}\right) \begin{pmatrix} 0 \\ 0 \\ fc_\beta \end{pmatrix}, \quad (2)$$

$$\Phi_2 = \exp\left(\frac{i\Theta'}{f}\right) \exp\left(-\frac{i\Theta}{ft_\beta}\right) \begin{pmatrix} 0 \\ 0 \\ fs_\beta \end{pmatrix}. \quad (3)$$

Here we have introduced the shorthand notation $s_\beta \equiv \sin \beta$, $c_\beta \equiv \cos \beta$, $t_\beta \equiv \tan \beta$. f is the Goldstone decay constant. Θ and Θ' are 3×3 matrix fields, parametrized as

$$\Theta = \frac{\eta}{\sqrt{2}} + \begin{pmatrix} \mathbf{0}_{2 \times 2} & h \\ h^\dagger & 0 \end{pmatrix}, \quad \Theta' = \frac{\zeta}{\sqrt{2}} + \begin{pmatrix} \mathbf{0}_{2 \times 2} & k \\ k^\dagger & 0 \end{pmatrix}. \quad (4)$$

η is the pseudoaxion, and h and k are parametrized as [v denotes the vacuum expectation value (VEV) of the Higgs doublet]

$$h = \begin{pmatrix} h^0 \\ h^- \end{pmatrix}, \quad h^0 = \frac{1}{\sqrt{2}}(v + H - i\chi), \quad (5)$$

$$k = \begin{pmatrix} k^0 \\ k^- \end{pmatrix}, \quad k^0 = \frac{1}{\sqrt{2}}(\sigma - i\omega). \quad (6)$$

For future convenience, we introduce the notation

$$\hat{h} \equiv (h^\dagger h)^{1/2}. \quad (7)$$

We note that the spontaneous global symmetry breaking (1) should deliver ten Goldstone bosons, which are parametrized here in terms of Θ and Θ' . The electroweak gauge group $SU(3)_L \times U(1)_X$ will eventually break to $U(1)_{EM}$, and therefore eight Goldstone bosons will be eaten to make the associated gauge bosons massive. Only two Goldstone bosons remain physical, denoted here as h and η . The parametrization of these Goldstone fields actually has some freedom; we refer the reader to Ref. [19] for an explanation.

In the SLH, under the full gauge group $SU(3)_C \times SU(3)_L \times U(1)_X$, Φ_1 and Φ_2 have quantum number $(\mathbf{1}, \mathbf{3})_{-\frac{1}{3}}$. The gauge kinetic term of Φ_1 and Φ_2 can thus be written as³

$$\mathcal{L}_{gk} = (D_\mu \Phi_1)^\dagger (D^\mu \Phi_1) + (D_\mu \Phi_2)^\dagger (D^\mu \Phi_2), \quad (8)$$

in which the covariant derivative can be expressed as⁴

$$D_\mu = \partial_\mu - igA_\mu^a T^a + ig_x Q_x B_\mu^x, \quad g_x = \frac{gt_W}{\sqrt{1 - t_W^2/3}}. \quad (9)$$

³We note that Eq. (8) automatically satisfies the requirement of CSB.

⁴In this paper our convention agrees with Ref. [23] but differs from Ref. [24]. The conversion between the two conventions is discussed in Appendix A.

In the above equation, A_μ^a and B_μ^x denote $SU(3)_L$ and $U(1)_X$ gauge fields, respectively. g and g_x denote the coupling constants of $SU(3)_L$ and $U(1)_X$ gauge groups, respectively. It is convenient to trade g_x for $t_W \equiv \tan \theta_W$. $T^a = \frac{\lambda^a}{2}$ where λ^a , $a = 1, \dots, 8$ denote the Gell-Mann matrices. For Φ_1 , Φ_2 , $Q_x = -\frac{1}{3}$. Following Ref. [23], we parametrize the $SU(3)_L$ gauge bosons as

$$A_\mu^a T^a = \frac{A_\mu^3}{2} \begin{pmatrix} 1 & 0 & 0 \\ 0 & -1 & 0 \\ 0 & 0 & 0 \end{pmatrix} + \frac{A_\mu^8}{2\sqrt{3}} \begin{pmatrix} 1 & 0 & 0 \\ 0 & 1 & 0 \\ 0 & 0 & -2 \end{pmatrix} + \frac{1}{\sqrt{2}} \begin{pmatrix} 0 & W_\mu^+ & Y_\mu^0 \\ W_\mu^- & 0 & X_\mu^- \\ Y_\mu^{0\dagger} & X_\mu^+ & 0 \end{pmatrix}, \quad (10)$$

with the *first-order* neutral gauge boson mixing relation ($c_W \equiv \cos \theta_W$, $s_W \equiv \sin \theta_W$)

$$\begin{pmatrix} A^3 \\ A^8 \\ B^x \end{pmatrix} = \begin{pmatrix} 0 & c_W & -s_W \\ \sqrt{1 - \frac{t_W^2}{3}} & \frac{s_W t_W}{\sqrt{3}} & \frac{s_W}{\sqrt{3}} \\ -\frac{t_W}{\sqrt{3}} & s_W \sqrt{1 - \frac{t_W^2}{3}} & c_W \sqrt{1 - \frac{t_W^2}{3}} \end{pmatrix} \begin{pmatrix} Z' \\ Z \\ A \end{pmatrix}. \quad (11)$$

Since the electroweak gauge group is enlarged to $SU(3)_L \times U(1)_X$, it is also necessary to enlarge the fermion sector in order that fermions transform properly under the enlarged group. We adopt the elegant anomaly-free embedding proposed in Refs. [16,25,26]. In the lepton Yukawa sector, the SM left-handed lepton doublets are enlarged to $SU(3)_L$ triplets $L_m = (\nu_L, \ell_L, iN_L)_m^T$ with $Q_x = -\frac{1}{3}$ ($m = 1, 2, 3$ is the family index). There are also right-handed singlet lepton fields ℓ_{Rm} with $Q_x = -1$ and N_{Rm} with $Q_x = 0$. The lepton Yukawa Lagrangian can be written as [23]

$$\mathcal{L}_{LY} = i\lambda_N^m \bar{N}_{Rm} \Phi_2^\dagger L_m + \frac{i\lambda_\ell^{mn}}{\Lambda} \bar{\ell}_{Rm} \epsilon_{ijk} \Phi_1^i \Phi_2^j L_n^k + \text{H.c.} \quad (12)$$

In the quark sector, we have the following field content:

$$Q_1 = (d_L, -u_L, iD_L)^T, \quad d_R, \quad u_R, \quad D_R, \quad (13)$$

$$Q_2 = (s_L, -c_L, iS_L)^T, \quad s_R, \quad c_R, \quad S_R, \quad (14)$$

$$Q_3 = (t_L, b_L, iT_L)^T, \quad t_R, \quad b_R, \quad T_R. \quad (15)$$

Here Q_1 , Q_2 transform under the $\bar{\mathbf{3}}$ representation of $SU(3)_L$ with $Q_x = 0$. Q_3 transforms under the $\mathbf{3}$ representation of $SU(3)_L$ with $Q_x = \frac{1}{3}$. The right-handed quark fields are all $SU(3)_L$ singlets with various $U(1)_X$ charges.

More specifically, u_R, c_R, t_R, T_R carry $Q_x = \frac{2}{3}$ while d_R, s_R, b_R, D_R, S_R carry $Q_x = -\frac{1}{3}$. The quark Yukawa Lagrangian can be written as [23]

$$\begin{aligned} \mathcal{L}_{QY} = & i\lambda_1^t \bar{u}_{R3}^1 \Phi_1^\dagger Q_3 + i\lambda_2^t \bar{u}_{R3}^2 \Phi_2^\dagger Q_3 \\ & + i \frac{\lambda_b^m}{\Lambda} \bar{d}_{Rm} \epsilon_{ijk} \Phi_1^i \Phi_2^j Q_3^k + i\lambda_1^{dn} \bar{d}_{Rn}^1 Q_n^T \Phi_1 \\ & + i\lambda_2^{dn} \bar{d}_{Rn}^2 Q_n^T \Phi_2 + i \frac{\lambda_u^{mn}}{\Lambda} \bar{u}_{Rm} \epsilon_{ijk} \Phi_1^{*i} \Phi_2^{*j} Q_n^k + \text{H.c.} \end{aligned} \quad (16)$$

In the above equation, $n = 1, 2$ is the family index for the first two generations of quark triplets. d_{Rm} runs over $(d_R, s_R, b_R, D_R, S_R)$ and u_{Rm} runs over (u_R, c_R, t_R, T_R) . u_{R3}^1, u_{R3}^2 are linear combinations of t_R and T_R . d_{Rn}^1, d_{Rn}^2 are linear combinations of d_R and D_R for $n = 1$ and of s_R and S_R for $n = 2$. It is worth noting that in the dimension-four part of Eqs. (12) and (16) CSB is formally preserved. In contrast, in Eqs. (12) and (16), the dimension-five part formally violates CSB. Nevertheless, the amount of violation is proportional to light fermion Yukawas and is thus negligible.

We now turn to the scalar potential. Using a CEFT approach and combining tree-level⁵ and one-loop contributions, the scalar effective potential in the SLH is calculated to be [19]

$$V = -\mu^2 (\Phi_1^\dagger \Phi_2 + \Phi_2^\dagger \Phi_1) + \lambda |\Phi_1^\dagger \Phi_2|^2 + \Delta(\hat{h}) \hat{h}^4. \quad (17)$$

μ^2 and λ could be regarded as parameters to be determined from experiments, while $\Delta(\hat{h})$ is automatically finite, and could be expressed in terms of the Lagrangian parameters in the model,

$$\begin{aligned} \Delta(\hat{h}) = & \frac{3}{16\pi^2} \left\{ \lambda_t^4 \left[\ln \frac{M_T^2}{m_t^2(\hat{h})} - \frac{1}{2} \right] \right. \\ & - \frac{1}{8} g^4 \left[\ln \frac{M_X^2}{m_W^2(\hat{h})} - \frac{1}{2} \right] \\ & \left. - \frac{1}{16} g^4 (1 + t_W^2)^2 \left[\ln \frac{M_{Z'}^2}{m_Z^2(\hat{h})} - \frac{1}{2} \right] \right\}. \end{aligned} \quad (18)$$

λ_t is defined as

$$\lambda_t \equiv \frac{\lambda_1^t \lambda_2^t}{\sqrt{\lambda_1^2 c_\beta^2 + \lambda_2^2 s_\beta^2}}, \quad (19)$$

⁵At tree level we do not include a $(\Phi_1^\dagger \Phi_2)^2 + \text{H.c.}$ term because it formally violates CSB. We note that introducing such a term may lead to spontaneous CP violation [27]. Furthermore, if both the $(\Phi_1^\dagger \Phi_2)^2 + \text{H.c.}$ term and Majorana mass terms for N_R 's are introduced, the SLH light neutrino masses can be radiatively generated [28].

where λ_1^t, λ_2^t are the two Yukawa couplings in the top sector, introduced in Eq. (16). $M_T^2, M_X^2, M_{Z'}^2$ are defined as

$$M_T^2 \equiv (\lambda_1^2 c_\beta^2 + \lambda_2^2 s_\beta^2) f^2, \quad (20)$$

$$M_X^2 \equiv \frac{1}{2} g^2 f^2, \quad (21)$$

$$M_{Z'}^2 \equiv \frac{2}{3 - t_W^2} g^2 f^2. \quad (22)$$

They are related to the physical mass squared of the relevant particles as follows:

$$M_T^2 = m_T^2 + m_t^2, \quad (23)$$

$$M_X^2 = m_X^2 + m_W^2, \quad (24)$$

$$M_{Z'}^2 = m_{Z'}^2 + m_Z^2, \quad (25)$$

in which m_T, m_t denote the physical mass of the heavy top T and the top quark t , m_X, m_W denote the physical mass of the X boson and W boson, and $m_{Z'}, m_Z$ denote the physical mass of the Z' boson and Z boson, respectively. $m_t^2(\hat{h}), m_W^2(\hat{h}), m_Z^2(\hat{h})$ are field-dependent masses squared, for which we use the following leading-order (LO) expressions:

$$m_t^2(\hat{h}) = \lambda_t^2 \hat{h}^2, \quad (26)$$

$$m_W^2(\hat{h}) = \frac{1}{2} g^2 \hat{h}^2, \quad (27)$$

$$m_Z^2(\hat{h}) = \frac{1}{2} g^2 (1 + t_W^2) \hat{h}^2. \quad (28)$$

With the above expressions for the scalar effective potential we are able to compute the electroweak VEV, Higgs mass, pseudoaxion mass, etc., as functions of μ^2, λ , and other Lagrangian parameters in the model.

Finally, we note that there of course exists a gauge-invariant kinetic Lagrangian for the $SU(3)_L \times U(1)_X$ gauge fields and the fermion fields in the model, according to their representations.

B. Hidden mass relation, unitarity, and naturalness

Before starting the phenomenological analysis in the SLH, it is important to notice that there exist certain constraints that we have to take into account [19].

First, there exists a hidden mass relation which follows from an analysis of the scalar effective potential (17). This is because if we consider g, t_W, λ_t as fixed, then the scalar effective potential (17) is fully determined by five parameters, say, $\mu^2, \lambda, f, t_\beta, m_T$. Requiring the electroweak VEV to be 246 GeV and the CP -even Higgs mass to be 125 GeV should eliminate two parameters, leaving only three

parameters as independent. For instance, we may choose f , t_β , m_T as the three independent parameters; then, any other observable could be expressed in terms of these three parameters. In particular, the pseudoaxion mass m_η is determined from the following hidden mass relation derived in Ref. [19]:

$$m_\eta^2 = [m_h^2 - v^2 \Delta_A (3 - 2\theta t_{2\theta}^{-1}) + v^2 A (5 - 2\theta t_{2\theta}^{-1})] s_\theta^{-2}. \quad (29)$$

Here $t_{2\theta}^{-1} \equiv \frac{1}{\tan(2\theta)}$, $s_\theta^{-2} \equiv \frac{1}{\sin^2\theta}$, and θ , A , Δ_A are defined by

$$\theta \equiv \frac{v}{\sqrt{2} f s_\beta c_\beta}, \quad (30)$$

$$A \equiv \frac{3}{16\pi^2} \left[\lambda_t^4 - \frac{g^4}{8} - \frac{g^4}{16} (1 + t_W^2)^2 \right], \quad (31)$$

$$\Delta_A \equiv \frac{3}{16\pi^2} \left[\lambda_t^4 \ln \frac{M_T^2}{m_t^2} - \frac{g^4}{8} \ln \frac{M_X^2}{m_W^2} - \frac{g^4}{16} (1 + t_W^2)^2 \ln \frac{M_{Z'}^2}{m_Z^2} \right]. \quad (32)$$

The basic feature of this mass relation is that the pseudoaxion mass is anticorrelated with the top partner mass.

Second, the SLH is meant to be only an effective field theory valid up to some energy scale, which could be revealed by an analysis of partial-wave unitarity. This was done in Ref. [19] and the unitarity cutoff was determined to be

$$\Lambda_U = \sqrt{8\pi} \times \min\{f c_\beta, f s_\beta\}. \quad (33)$$

Apart from the lepton Yukawa part, the SLH Lagrangian is manifestly symmetric with respect to the exchange $\Phi_1 \leftrightarrow \Phi_2$ (with the corresponding exchange of all related coefficients), and therefore without loss of generality we may restrict to $t_\beta \geq 1$. The resulting formulas have the $t_\beta \leftrightarrow \frac{1}{t_\beta}$ invariance. Nevertheless, the lepton Yukawa Lagrangian (12) does not share this exchange symmetry, and the $t_\beta \leftrightarrow \frac{1}{t_\beta}$ invariance could be lost. However, if we do not deal directly with lepton-related vertices, the $t_\beta \leftrightarrow \frac{1}{t_\beta}$ invariance violation could only come from input parameter corrections, which are all suppressed by $\frac{v^2}{f^2}$ [19], which is a very small quantity if we consider current bounds on f . Therefore in the following, unless otherwise specified, we will assume $t_\beta \geq 1$. (Moreover, in Sec. IV we will show that the $t_\beta < 1$ case is disfavored by electroweak precision measurements for natural regions of parameter space.) Then we can express the unitarity cutoff as

$$\Lambda_U = \sqrt{8\pi} f c_\beta \quad (34)$$

and we require all particle masses be less than Λ_U . We note that since Λ_U is determined by the smaller of the triplet VEVs, while $m_{Z'}$ is determined by the quadrature of the triplet VEVs, requiring $m_{Z'} \leq \Lambda_U$ leads to an upper bound on t_β (besides our assumption $t_\beta \geq 1$)

$$1 \leq t_\beta \leq \sqrt{\frac{4\pi(3 - t_W^2)}{g^2}} - 1 \approx 8.9. \quad (35)$$

Third, the parameter M_T has a lower bound derived simply from the structure of the Yukawa Lagrangian [24]

$$M_T \geq \sqrt{2} \frac{m_t}{v} f s_{2\beta} \approx f s_{2\beta}, \quad (36)$$

where $s_{2\beta} \equiv \sin(2\beta)$. M_T is also bounded from above by either Λ_U or the requirement that m_η^2 obtained from Eq. (29) should be positive.

Finally, from the LHC search for the Z' boson in the dilepton channel [29,30], we estimate the lower bound on f as [27]

$$f \gtrsim 7.5 \text{ TeV}, \quad (37)$$

We note that when combined with Eqs. (36) and (35) this also leads to a lower bound on the top partner mass of around 1.7 TeV, which is much more stringent than constraints from top partner searches at the LHC.

It is remarkable that the naturalness issue can also be analyzed in a CEFT approach, which was done in Ref. [19]. We define the total degree of fine-tuning at a certain parameter point as

$$\Delta_{\text{TOT}} = \max\{\Delta_{\text{TOT}}^{\mu^2}, \Delta_{\text{TOT}}^\lambda\}, \quad (38)$$

where $\Delta_{\text{TOT}}^{\mu^2}$, $\Delta_{\text{TOT}}^\lambda$ are defined by

$$\Delta_{\text{TOT}}^\lambda \equiv \left| \frac{\lambda_U}{m_h^2} \frac{\partial m_h^2}{\partial \lambda_U} \right|, \quad \Delta_{\text{TOT}}^{\mu^2} \equiv \left| \frac{\mu_U^2}{m_h^2} \frac{\partial m_h^2}{\partial \mu_U^2} \right|. \quad (39)$$

Here λ_U , μ_U^2 denote the λ , μ^2 parameters defined at the unitarity cutoff. The above definitions obviously reflect how the IR parameters (e.g., m_h^2) are sensitive to UV parameters (e.g., λ_U , μ_U^2), and thus may serve as a measure of the degree of fine-tuning in the allowed parameter space. We may follow Ref. [19] to compute the degree of fine-tuning, and find several general features. One feature which is easy to understand is, generally speaking, with smaller f and m_T we could get a smaller degree of fine-tuning.

In Fig. 1 we present the density plot of $\text{Log}\Delta_{\text{TOT}}$ in the m_η - m_T plane for $f = 8$ TeV. Only the colored region is allowed by various constraints. From the figure it is clear that the parameter region favored by naturalness considerations is featured by a small m_T , with m_η around 500 GeV. A light η , with a mass less than $2m_t$, is unfortunately disfavored.

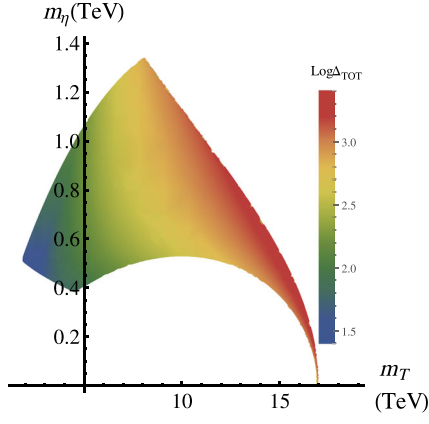


FIG. 1. Density plot of $\text{Log}\Delta_{\text{TOT}}$ in the m_η - m_T plane for $f = 8$ TeV. Log means \log_{10} .

C. Fermion mass diagonalization and flavor assumption

Fermion mass diagonalization has been studied in Refs. [23,24]. In the lepton sector, the fermion mass matrices can be diagonalized by the following field rotations:

$$\begin{pmatrix} N_{Ln} \\ \nu_{Ln} \end{pmatrix} \rightarrow \begin{pmatrix} c_\delta & s_\delta \\ s_\delta & -c_\delta \end{pmatrix} \begin{pmatrix} N_{Ln} \\ \nu_{Ln} \end{pmatrix}, \quad n = 1, 2, 3, \quad \delta \equiv \frac{v}{\sqrt{2}f t_\beta}, \quad (40)$$

$$\begin{pmatrix} e_L \\ \mu_L \\ \tau_L \end{pmatrix} \rightarrow U_l \begin{pmatrix} e_L \\ \mu_L \\ \tau_L \end{pmatrix}, \quad \begin{pmatrix} e_R \\ \mu_R \\ \tau_R \end{pmatrix} \rightarrow W_l \begin{pmatrix} e_R \\ \mu_R \\ \tau_R \end{pmatrix}, \quad (41)$$

where U_l, W_l are both 3×3 unitary matrices. In this work, for simplicity we will assume that U_l, W_l are both identity matrices. This leads to a simplification of some Feynman rules associated with the heavy neutrino N .

In the quark sector, first of all we perform field rotations in the right-handed sector as follows:

$$u_{R3}^1 = \frac{-\lambda_2^t s_\beta t_R + \lambda_1^t c_\beta T_R}{\sqrt{\lambda_1^t c_\beta^2 + \lambda_2^t s_\beta^2}}, \quad u_{R3}^2 = \frac{\lambda_1^t c_\beta t_R + \lambda_2^t s_\beta T_R}{\sqrt{\lambda_1^t c_\beta^2 + \lambda_2^t s_\beta^2}}, \quad (42)$$

$$d_{R1}^1 = \frac{-\lambda_2^d s_\beta d_R + \lambda_1^d c_\beta D_R}{\sqrt{\lambda_1^d c_\beta^2 + \lambda_2^d s_\beta^2}}, \quad d_{R1}^2 = \frac{\lambda_1^d c_\beta d_R + \lambda_2^d s_\beta D_R}{\sqrt{\lambda_1^d c_\beta^2 + \lambda_2^d s_\beta^2}}, \quad (43)$$

$$d_{R2}^1 = \frac{-\lambda_2^s s_\beta s_R + \lambda_1^s c_\beta S_R}{\sqrt{\lambda_1^s c_\beta^2 + \lambda_2^s s_\beta^2}}, \quad d_{R2}^2 = \frac{\lambda_1^s c_\beta s_R + \lambda_2^s s_\beta S_R}{\sqrt{\lambda_1^s c_\beta^2 + \lambda_2^s s_\beta^2}}. \quad (44)$$

For simplicity, the phenomenological studies done in this work will be carried out under the following flavor assumptions on the quark Yukawa Lagrangian (16):

$$\lambda_u^{Tu} = \lambda_u^{Tc} = \lambda_u^{12} = \lambda_u^{21} = \lambda_u^{31} = \lambda_u^{32} = 0, \quad (45)$$

$$\lambda_b^D = \lambda_b^S = \lambda_b^1 = \lambda_b^2 = 0. \quad (46)$$

These flavor assumptions turn off all of the generation-crossing quark flavor transitions and lead to a trivial Cabibbo-Kobayashi-Maskawa matrix, i.e., $V_{\text{CKM}} = \mathbf{1}_{3 \times 3}$, which is not realistic. Nevertheless, in this paper we are concerned with the direct production of new physics particles at high-energy colliders rather than quark flavor observables. Also, for the parameter region that we are interested in, the phenomenology is not sensitive to the flavor assumptions adopted here, if the λ 's in Eqs. (45) and (46), which characterize the generation-crossing quark flavor changing effects, are small.

With the above flavor assumptions, it is then straightforward to show that, up to $\mathcal{O}(\frac{v}{f})$, after right-handed sector field rotations we only need to perform the following field rotations in the left-handed sector to diagonalize the quark mass matrices:

$$\begin{pmatrix} t_L \\ T_L \end{pmatrix} \rightarrow \begin{pmatrix} 1 & -\delta_t \\ \delta_t & 1 \end{pmatrix} \begin{pmatrix} t_L \\ T_L \end{pmatrix}, \quad (47)$$

$$\begin{pmatrix} d_L \\ D_L \end{pmatrix} \rightarrow \begin{pmatrix} 1 & -\delta_{Dd} \\ \delta_{Dd} & 1 \end{pmatrix} \begin{pmatrix} d_L \\ D_L \end{pmatrix}, \quad (48)$$

$$\begin{pmatrix} s_L \\ S_L \end{pmatrix} \rightarrow \begin{pmatrix} 1 & -\delta_{Ss} \\ \delta_{Ss} & 1 \end{pmatrix} \begin{pmatrix} s_L \\ S_L \end{pmatrix}. \quad (49)$$

In the above equations, the field rotation parameters $\delta_t, \delta_{Dd}, \delta_{Ss}$ can be expressed using f, β and the corresponding heavy fermion mass as follows⁶:

$$\delta_t = \frac{v}{2\sqrt{2}f s_\beta c_\beta} \left(s_\beta^2 - c_\beta^2 \pm \sqrt{1 - 8 \frac{m_t^2}{v^2} \frac{f^2}{M_T^2} s_\beta^2 c_\beta^2} \right), \quad (50)$$

$$\delta_{Dd} = -\frac{v}{2\sqrt{2}f s_\beta c_\beta} \left(s_\beta^2 - c_\beta^2 \pm \sqrt{1 - 8 \frac{m_d^2}{v^2} \frac{f^2}{M_D^2} s_\beta^2 c_\beta^2} \right), \quad (51)$$

$$\delta_{Ss} = -\frac{v}{2\sqrt{2}f s_\beta c_\beta} \left(s_\beta^2 - c_\beta^2 \pm \sqrt{1 - 8 \frac{m_s^2}{v^2} \frac{f^2}{M_S^2} s_\beta^2 c_\beta^2} \right). \quad (52)$$

⁶Our expressions for $\delta_t, \delta_{Dd}, \delta_{Ss}$ differ from the corresponding expressions in Eq. (2.63) of Ref. [23]. The expressions of $\delta_t, \delta_{Dd}, \delta_{Ss}$ given in Ref. [23] are not consistent with their counterparts in Ref. [24]. Our calculation agrees with Ref. [24].

Note that in the above equations, before the square root, both the plus sign and minus sign give possible solutions, which leads to a total of eight sign combinations. When we refer to the sign combination in these equations, we will list them according to the order $\delta_r, \delta_{Dd}, \delta_{Ss}$, as, e.g., $(+, +, +)$, $(+, +, -)$, etc., m_d, m_s, M_D, M_S correspond to the mass of d, s, D, S , respectively. In the following we will simply neglect the small m_d, m_s ; then, the expressions of δ_{Dd}, δ_{Ss} become identical, apart from a possible sign difference before the square root. Then, we obtain the simple expression

$$\delta_{Dd}^+ = \delta_{Ss}^+ = -\frac{vt_\beta}{\sqrt{2}f}, \quad \delta_{Dd}^- = \delta_{Ss}^- = \frac{v}{\sqrt{2}ft_\beta}, \quad (53)$$

where the superscripts indicate the sign choice for the corresponding rotation parameter. The rotation parameters $\delta_r, \delta_{Dd}, \delta_{Ss}$ are important since they appear directly in the coefficients of various interaction vertices which affect the η phenomenology, as we will see.

D. Lagrangian in the mass basis

We are now prepared to present the Lagrangian in the mass basis which is relevant for the investigation of η phenomenology. However, let us first note that there is a subtle issue regarding the diagonalization in the bosonic sector. After EWSB, it can be shown that the CP -odd sector scalar kinetic matrix in terms of the $\eta, \zeta, \chi, \omega$ fields is not canonically normalized. Also, there exist ‘‘unexpected’’ two-point vector-scalar transition terms like $Z^\mu \partial_\mu \eta$ after expanding the covariant derivative terms of the scalar fields. Therefore, a further field rotation (including a proper gauge fixing) is needed to diagonalize the bosonic sector. This subtle issue had been overlooked for a long time in the literature, and was only remedied in a recent paper [22]. In Ref. [22], an expression for the fraction of mass eigenstate η field contained in the $\eta, \zeta, \chi, \omega$ fields originally introduced in the parametrization (4)–(6) was obtained, valid to all orders in $\xi \equiv \frac{v}{f}$, as follows (we collect the four fraction values into a four-component column vector Υ):

$$\Upsilon = \begin{pmatrix} c_{\gamma+\delta}^{-1} \\ -c_{\gamma+\delta}^{-1}(s_\delta^2 t_\beta - s_\gamma^2 t_\beta^{-1}) \\ \frac{v}{\sqrt{2}f} c_{\gamma+\delta}^{-1}(c_{2\delta} t_\beta - c_{2\gamma} t_\beta^{-1}) \\ \frac{1}{2} c_{\gamma+\delta}^{-1}(s_{2\delta} t_\beta + s_{2\gamma} t_\beta^{-1}) \end{pmatrix}, \quad (54)$$

where

$$\gamma \equiv \frac{vt_\beta}{\sqrt{2}f}, \quad \delta \equiv \frac{v}{\sqrt{2}ft_\beta}. \quad (55)$$

The Υ vector is involved in the derivation of all η -related mass eigenstate vertices. In particular, from the expression of Υ we see that there is an $\mathcal{O}(\xi)$ component of the mass eigenstate η contained in χ . This has the following consequences. If we parametrize the mass eigenstate $ZH\eta$ vertex as

$$\begin{aligned} \mathcal{L}_{ZH\eta} &= c_{ZH\eta}^{as} Z^\mu (\eta \partial_\mu H - H \partial_\mu \eta) \\ &\quad + c_{ZH\eta}^s Z^\mu (\eta \partial_\mu H + H \partial_\mu \eta), \end{aligned} \quad (56)$$

where $c_{ZH\eta}^{as}$ denotes the coefficient of the antisymmetric $ZH\eta$ vertex, and $c_{ZH\eta}^s$ denotes the coefficient of the symmetric $ZH\eta$ vertex, then it was shown in Ref. [22] that

$$c_{ZH\eta}^{as} = -\frac{g}{4\sqrt{2}c_W^3 t_{2\beta}} \xi^3 + \mathcal{O}(\xi^5), \quad (57)$$

$$\begin{aligned} c_{ZH\eta}^s &= \frac{g}{\sqrt{2}c_W t_{2\beta}} \xi + \frac{g}{24\sqrt{2}c_W s_{2\beta}} \left[\frac{8}{s_{2\beta} t_{2\beta}} \right. \\ &\quad \left. + 3c_{2\beta} \left(8 + \frac{6}{c_W^2} - \frac{1}{c_W^4} \right) \right] \xi^3 + \mathcal{O}(\xi^5). \end{aligned} \quad (58)$$

We see that the antisymmetric $ZH\eta$ vertex only shows up from $\mathcal{O}(\xi^3)$, in contrast to the results presented in Refs. [17,18] which claimed the existence of antisymmetric $ZH\eta$ vertex at $\mathcal{O}(\xi)$ due to the lack of an appropriate diagonalization in the bosonic sector.

This subtle issue of diagonalization in the bosonic sector also has an impact on the η coupling to fermions. For instance, if we consider the expansion of $\epsilon_{ijk} \Phi_1^i \Phi_2^j$, with the help of the expression for the Υ vector in Eq. (54), we could find the following result for the neutral component:

$$\epsilon_{ijk} \Phi_1^i \Phi_2^j \supset -if \begin{pmatrix} 0 \\ fs_\beta c_\beta s_{\gamma+\delta} + \frac{1}{\sqrt{2}} c_{\gamma+\delta} H \\ 0 \end{pmatrix}. \quad (59)$$

An important message from this is that $\epsilon_{ijk} \Phi_1^i \Phi_2^j$ does not contain any fraction of the mass eigenstate η field, to all orders in ξ . Therefore, from Eq. (12) we immediately conclude that η does not couple to a pair of charged leptons to all orders in ξ . This point was overlooked in previous studies [21,31] which relied on $\eta \rightarrow \tau\tau$.

In the following, let us collect the other mass eigenstate vertices that are relevant for η phenomenology, to the first nontrivial order in ξ . In the Yukawa sector, we have the following couplings of H and η to a pair of fermions.

(1) H and η couplings to the lepton sector:

$$\begin{aligned} \mathcal{L}_{LY} \supset & -\sum_{n=1}^3 \frac{m_{ln}}{\sqrt{2}f s_\beta c_\beta t_{\gamma+\delta}} H \bar{l}_{Rn} l_{Ln} + \sum_{n=1}^3 \frac{M_{Nn}}{\sqrt{2}f t_\beta} H \bar{N}_{Rn} \nu_{Ln} \\ & - i \sum_{n=1}^3 \frac{M_{Nn}}{\sqrt{2}f t_\beta} c_{\gamma+\delta} \eta \bar{N}_{Rn} N_{Ln} - i \sum_{n=1}^3 \frac{M_{Nn}}{\sqrt{2}f t_\beta} s_{\gamma+\delta} \eta \bar{N}_{Rn} \nu_{Ln} + \text{H.c.} \end{aligned} \quad (60)$$

(2) H and η couplings to the up-type quark sector:

$$\begin{aligned} \mathcal{L}_{QY} \supset & -\frac{m_u}{v} H \bar{u}_R u_L - \frac{m_c}{v} H \bar{c}_R c_L \\ & - \frac{m_t}{v} H \bar{t}_R t_L + \frac{m_t}{v} \left(\frac{\sqrt{2}v}{f t_{2\beta}} + \delta_t \right) H \bar{t}_R T_L + \frac{M_T}{v} \delta_t H \bar{T}_R t_L + \frac{m_t^2}{v M_T} H \bar{T}_R T_L \\ & - i \frac{m_t}{v} \delta_t \eta \bar{t}_R t_L - i \frac{m_t}{v} \eta \bar{t}_R T_L + i \frac{M_T}{v} \left(\frac{v^2}{2f^2} + \delta_t^2 \right) \eta \bar{T}_R t_L + i \frac{M_T}{v} \delta_t \eta \bar{T}_R T_L + \text{H.c.} \end{aligned} \quad (61)$$

(3) H and η couplings to the down-type quark sector:

$$\begin{aligned} \mathcal{L}_{QY} \supset & -\frac{m_b}{v} H \bar{b}_R b_L \\ & - \frac{m_d}{v} H \bar{d}_R d_L + \frac{m_d}{v} \left(-\frac{\sqrt{2}v}{f t_{2\beta}} + \delta_{Dd} \right) H \bar{d}_R D_L + \frac{M_D}{v} \delta_{Dd} H \bar{D}_R d_L + \frac{m_d^2}{v M_D} H \bar{D}_R D_L \\ & - \frac{m_s}{v} H \bar{s}_R s_L + \frac{m_s}{v} \left(-\frac{\sqrt{2}v}{f t_{2\beta}} + \delta_{Ss} \right) H \bar{s}_R S_L + \frac{M_S}{v} \delta_{Ss} H \bar{S}_R s_L + \frac{m_s^2}{v M_S} H \bar{S}_R S_L \\ & - i \frac{m_d}{v} \delta_{Dd} \eta \bar{d}_R d_L - i \frac{m_d}{v} \eta \bar{d}_R D_L + i \frac{M_D}{v} \left(\frac{v^2}{2f^2} + \delta_{Dd}^2 \right) \eta \bar{D}_R d_L + i \frac{M_D}{v} \delta_{Dd} \eta \bar{D}_R D_L \\ & - i \frac{m_s}{v} \delta_{Ss} \eta \bar{s}_R s_L - i \frac{m_s}{v} \eta \bar{s}_R S_L + i \frac{M_S}{v} \left(\frac{v^2}{2f^2} + \delta_{Ss}^2 \right) \eta \bar{S}_R s_L + i \frac{M_S}{v} \delta_{Ss} \eta \bar{S}_R S_L + \text{H.c.} \end{aligned} \quad (62)$$

In the above equations, m_{ln} , $n = 1, 2, 3$ denote the masses of e, μ, τ leptons, M_{Nn} , $n = 1, 2, 3$ denote the masses of the three heavy neutral leptons N_n , and m_u, m_c denote the masses of the u, c quarks, respectively. η can also be a decay product of the heavy fermions N, T, D, S , and therefore we also list the relevant Lagrangian for the heavy fermion gauge interaction which enters the heavy fermion decays,

$$\begin{aligned} \mathcal{L}_{\text{matter}} \supset & \frac{gv}{2ft_\beta} W_\mu^+ \bar{N}_{Lm} \gamma^\mu l_{Lm} - \frac{gv}{2\sqrt{2}c_W f t_\beta} Z_\mu \bar{N}_{Lm} \gamma^\mu \nu_{Lm} \\ & - \frac{g\delta_t}{\sqrt{2}} W_\mu^+ \bar{T}_L \gamma^\mu b_L - \frac{g\delta_t}{2c_W} Z_\mu \bar{T}_L \gamma^\mu t_L \\ & - \frac{g\delta_{Dd}}{\sqrt{2}} W_\mu^+ \bar{u}_L \gamma^\mu D_L + \frac{g\delta_{Dd}}{2c_W} Z_\mu \bar{d}_L \gamma^\mu D_L - \frac{g\delta_{Ss}}{\sqrt{2}} W_\mu^+ \bar{c}_L \gamma^\mu S_L + \frac{g\delta_{Ss}}{2c_W} Z_\mu \bar{s}_L \gamma^\mu S_L + \text{H.c.} \end{aligned} \quad (63)$$

A further interesting possibility is that η might come from the decay of a Z' boson. The Z' -related parts of the interaction Lagrangian are listed below.

(1) Z' couplings to leptons:

$$\begin{aligned} \mathcal{L}_{\text{matter}} \supset & g \frac{1-t_W^2}{2\sqrt{3-t_W^2}} \bar{l}_{Ln} \gamma^\mu l_{Ln} Z'_\mu - g \frac{t_W^2}{\sqrt{3-t_W^2}} \bar{l}_{Rn} \gamma^\mu l_{Rn} Z'_\mu \\ & + g \frac{1-t_W^2}{2\sqrt{3-t_W^2}} \bar{\nu}_{Ln} \gamma^\mu \nu_{Ln} Z'_\mu - g \frac{1}{\sqrt{3-t_W^2}} \bar{N}_{Ln} \gamma^\mu N_{Ln} Z'_\mu. \end{aligned} \quad (64)$$

(2) Z' couplings to third-generation quarks:

$$\begin{aligned} \mathcal{L}_{\text{matter}} \supset & -g \frac{3 - 2t_W^2}{3\sqrt{3 - t_W^2}} \bar{T}_L \gamma^\mu T_L Z'_\mu + g \frac{2t_W^2}{3\sqrt{3 - t_W^2}} \bar{T}_R \gamma^\mu T_R Z'_\mu \\ & + g \frac{3 + t_W^2}{6\sqrt{3 - t_W^2}} \bar{t}_L \gamma^\mu t_L Z'_\mu + g \frac{2t_W^2}{3\sqrt{3 - t_W^2}} \bar{t}_R \gamma^\mu t_R Z'_\mu \\ & + g \frac{3 + t_W^2}{6\sqrt{3 - t_W^2}} \bar{b}_L \gamma^\mu b_L Z'_\mu - g \frac{t_W^2}{3\sqrt{3 - t_W^2}} \bar{b}_R \gamma^\mu b_R Z'_\mu. \end{aligned} \quad (65)$$

(3) Z' couplings to first- and second-generation quarks:

$$\begin{aligned} \mathcal{L}_{\text{matter}} \supset & g \frac{\sqrt{3 - t_W^2}}{3} \bar{D}_L \gamma^\mu D_L Z'_\mu - g \frac{t_W^2}{3\sqrt{3 - t_W^2}} \bar{D}_R \gamma^\mu D_R Z'_\mu \\ & - g \frac{\sqrt{3 - t_W^2}}{6} \bar{d}_L \gamma^\mu d_L Z'_\mu - g \frac{t_W^2}{3\sqrt{3 - t_W^2}} \bar{d}_R \gamma^\mu d_R Z'_\mu \\ & - g \frac{\sqrt{3 - t_W^2}}{6} \bar{u}_L \gamma^\mu u_L Z'_\mu + g \frac{2t_W^2}{3\sqrt{3 - t_W^2}} \bar{u}_R \gamma^\mu u_R Z'_\mu \\ & + \text{terms with } u \rightarrow c, d \rightarrow s, D \rightarrow S. \end{aligned} \quad (66)$$

(4) Z' couplings to bosons (relevant for Z' decay):

$$\begin{aligned} \mathcal{L}_{\text{gauge}} \supset & -ig\sqrt{3 - t_W^2}(1 - t_W^2) \frac{v^2}{8f^2} \{(\partial_\mu Z'_\nu)(W^{-\mu}W^{+\nu} - W^{+\mu}W^{-\nu}) \\ & + Z'^\mu[(\partial_\mu W_\nu^+)W^{-\nu} - (\partial_\mu W_\nu^-)W^{+\nu}] + Z'^\nu[(\partial_\mu W_\nu^-)W^{+\mu} - (\partial_\mu W_\nu^+)W^{-\mu}]\}, \end{aligned} \quad (67)$$

$$\begin{aligned} \mathcal{L}_{gk} \supset & -\frac{\sqrt{2}gv}{\sqrt{3 - t_W^2}ft_{2\beta}} Z'^\mu(\eta\partial_\mu H - H\partial_\mu\eta) - \frac{\sqrt{3 - t_W^2}gv}{\sqrt{2}ft_{2\beta}} Z'^\mu(\eta\partial_\mu H + H\partial_\mu\eta) \\ & - \frac{g^2v}{2c_W^2\sqrt{3 - t_W^2}} \eta Z'^\mu \frac{(Y_\mu^{0\dagger} + Y_\mu^0)}{\sqrt{2}} + \frac{g^2vc_{2W}}{2c_W^3\sqrt{3 - t_W^2}} HZ'^\mu Z_\mu. \end{aligned} \quad (68)$$

III. SYMMETRIC VSS VERTICES

In the derivation of the SLH Lagrangian in the mass basis we obtained the $ZH\eta$ vertex in the form of Eq. (56), which contains two parts: the antisymmetric part $[Z^\mu(\eta\partial_\mu H - H\partial_\mu\eta)]$ and the symmetric part $[Z^\mu(\eta\partial_\mu H + H\partial_\mu\eta)]$.⁷ An antisymmetric VSS vertex often appears in models based on a linearly realized scalar sector, such as the usual two-Higgs-doublet model (2HDM). It is natural to ask whether the symmetric VSS vertices can have any

⁷The Hermiticity requirement on the Lagrangian does not forbid the symmetric part. Z_μ, H, η are all real fields. ∂_μ does not lead to an additional minus sign under Hermitian conjugation because in quantum field theory x^μ 's are labels, not operators. This is not to be confused with the situation in ordinary quantum mechanics.

physical effect. We note that in a Lorentz-invariant $ZH\eta$ vertex, the ∂_μ may act on any of the three fields (Z^μ, H, η). However because a total derivative term $\partial_\mu(Z^\mu H\eta)$ has no physical effects, we therefore expect at most two independent contributions from the interaction of one vector field with two scalar fields. If symmetric VSS vertices are allowed and present in a general theory and could lead to distinct physical effects, it would mean that a vector field could interact with two scalar fields in a manner different from the usually expected antisymmetric pattern, which may further reveal interesting features of the enlarged scalar sector.

Let us first note that the symmetric VSS Lagrangian $Z^\mu(\eta\partial_\mu H + H\partial_\mu\eta)$ can be written as

$$Z_\mu \partial^\mu (H\eta) \quad (69)$$

via Leibniz's rule and is therefore (via integration by parts) equivalent to

$$-(\partial^\mu Z_\mu)(H\eta) \quad (70)$$

in the Lagrangian formulation of the theory. A reflective reader might at this moment wonder whether terms like Eq. (70) indeed contribute to S -matrix elements if canonical quantization is adopted. Note that what matters in canonical quantization is the interaction Hamiltonian in the interaction picture (denoted H_I^{int}), and if Z^μ is a massive spin-1 field, then the corresponding interaction picture field operator Z_I^μ (the subscript “ I ” denotes interaction picture) will automatically satisfy [32]

$$\partial_\mu Z_I^\mu = 0. \quad (71)$$

It is tempting to arrive at the conclusion that terms like Eq. (70) cannot contribute to S -matrix elements due to Eq. (71). Actually, this is not quite correct. The correct procedure to go from the classical Lagrangian to the interaction Hamiltonian in the interaction picture H_I^{int} is to (i) identify appropriate canonical coordinates and their conjugate momenta, (ii) perform a Legendre transformation to obtain the Hamiltonian and express it in terms of canonical coordinates and their conjugate momenta, (iii) promote the canonical variables to field operators satisfying appropriate canonical commutation relations, and finally (iv) split the Hamiltonian into a free part and an interaction part and replace the Heisenberg-picture quantities with their interaction-picture counterparts [32]. If this procedure is strictly followed, we would find that only the spatial components of Z^μ can be treated as independent canonical coordinates while Z^0 is dependent because regardless of whether we start with Eq. (69) or Eq. (70) the derivative of the Lagrangian with respect to \dot{Z}_0 cannot be made to satisfy canonical commutation relations. To avoid the appearance of $\partial^0 Z_0$ in the Hamiltonian we could start with Eq. (69), and then the problem turns out to be the same as that treated in Sec. 7.5 of Ref. [32]. Using the results there, we could see that Eq. (69) leads to a term

$$-Z_I^\mu \partial_\mu (h_I A_I) \quad (72)$$

in the interaction Hamiltonian in the interaction picture (barring a Lorentz noncovariant term which is not shown here). This will certainly lead to a vertex Feynman rule

$$-k^\mu, \quad (73)$$

where k^μ is the Z momentum flowing into the vertex. This vertex Feynman rule could also be derived from Eq. (69) via the path-integral method. Notice that it is not legitimate to perform integration by parts in the interaction-picture Hamiltonian H_I^{int} to obtain

$$(\partial_\mu Z_I^\mu)(h_I A_I) \quad (74)$$

from Eq. (72).⁸

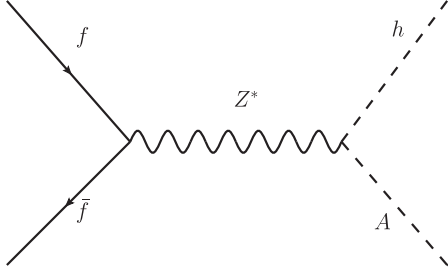
The appearance of $\partial_\mu Z^\mu$ in Eq. (70) is reminiscent of covariant gauge fixing in gauge field theories. Equation (70) is not gauge invariant; nevertheless, at this moment let us suppose that it can be deduced from a gauge-invariant operator. Because we are dealing with quantum field theories it is important not to confuse them with classical field theories. In a classical gauge field theory a gauge-fixing condition (such as the Landau gauge condition $\partial_\mu Z^\mu = 0$) is employed so that the solutions of the equation of motion are required to also satisfy the gauge-fixing condition. In quantum field theory all classical field configurations, regardless of whether they satisfy the classical equation of motion, are to be integrated over in the path integral. The usually adopted covariant gauge, the general R_ξ gauge, actually corresponds to a Gaussian smearing of a class of covariant gauge conditions and does not strictly force the classical field to satisfy a simple gauge-fixing equation. However, the limit $\xi \rightarrow 0$ makes the gauge-fixing functional act like a delta function imposing the Landau gauge condition $\partial_\mu Z^\mu = 0$ [32]. Therefore, it is heuristic to guess that in the Landau gauge, symmetric VSS vertices do not contribute to the S -matrix of the theory. However, we should not forget that in the Landau gauge it is necessary to take into account the Goldstone contribution to the S -matrix, and also the associated ghost contribution when we go beyond tree level in perturbation theory. This observation suggests that at tree level, processes involving symmetric VSS vertices can be seen as purely Goldstone mediated.

Physical effects of antisymmetric VSS vertices have been well studied in the literature. For example, in the 2HDM, a benchmark process which embodies the effect of antisymmetric VSS vertices is

$$f + \bar{f} \rightarrow A + h \quad (75)$$

where A and h denote a generic CP -odd and CP -even 2HDM Higgs boson, respectively. The corresponding Feynman diagram is shown in Fig. 2 in unitarity gauge. Now suppose we replace the antisymmetric VSS ZhA vertex in Fig. 2 by a completely symmetric VSS ZhA vertex. It is obvious that if the Z boson is on shell, then the amplitude should vanish since for an on-shell massive vector boson we have the relation $p \cdot \epsilon = 0$ for its

⁸More specifically, integration by parts for spatial components of H_I^{int} should be fine if the fields are assumed to satisfy certain boundary conditions, which is usually the case. However, integration by parts for the temporal component of H_I^{int} is problematic since in the expression for the scattering operator $S = T \exp(-i \int_{-\infty}^{+\infty} H_I^{\text{int}} dt)$ the temporal integration is actually twisted by the time ordering. No such problem exists if we adopt the path-integral method.

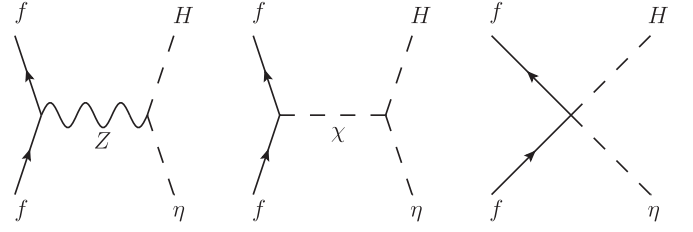
FIG. 2. Associated production of h and A .

momentum and polarization vectors. It is tempting to proceed with the case where the Z boson is off shell. The amplitude in this case can be examined from two perspectives. First, we can perform the calculation in unitarity gauge. In this gauge, the result of dotting the Z momentum p at the ZhA vertex into its s -channel propagator is again proportional to the Z momentum p at the $Zf\bar{f}$ vertex. It is then obvious that only the axial-vector part of the $Zf\bar{f}$ vertex contributes to the amplitude, with a contribution proportional to the fermion mass m_f . Alternatively, we may perform the calculation in Landau gauge ($\xi = 0$), in which the diagram shown in Fig. 2 does not contribute to the amplitude; nevertheless, we need to take into account the s -channel Goldstone-mediated amplitude, which again gives a contribution proportional to the fermion mass m_f .

Although usually f is a light fermion with negligible mass effects, we might be interested in the case where f is heavy with important mass effects, e.g., the top quark. If in this case the symmetric VSS vertex could lead to physical effects, we would seem to produce a paradox in the SLH. In the SLH there exists a symmetric $ZH\eta$ vertex; however, if we consider a linearly realized SLH as a UV completion, then it cannot lead to symmetric VSS vertices and hence there will be no related physical effects. Since the usual nonlinearly realized SLH can be related to a linearly realized SLH via an appropriate field redefinition, the above discussion seems to violate the field redefinition invariance of the S -matrix element.⁹ We can turn the argument around to use the field redefinition invariance to infer the existence of an additional contribution in the SLH which also contributes to the $f\bar{f} \rightarrow H\eta$ process such that the field redefinition invariance is maintained. In fact, if we examine the Yukawa part of the SLH Lagrangian, we would find the following four-point contact vertex (m_f denotes the mass of f):

$$\mathcal{L} \supset i \frac{2\sqrt{2}g_A m_f}{ft_{2\beta} v} H\eta\bar{f}\gamma^5 f. \quad (76)$$

⁹The radial mode does not help since it does not have the required CP property.

FIG. 3. Feynman diagrams in the SLH for $f\bar{f} \rightarrow H\eta$ in R_ξ gauge.

Here g_A is the axial coupling of the fermion f which also appears in its interaction with the Z boson and the associated Goldstone χ as

$$\mathcal{L} \supset \frac{g}{2c_W} Z^\mu \bar{f}\gamma_\mu (g_V + g_A\gamma^5) f + i \frac{2g_A m_f}{v} \bar{f}\gamma^5 f \chi. \quad (77)$$

Now if we compute the amplitude for $f\bar{f} \rightarrow H\eta$ in R_ξ gauge, we need to include three contributions: s -channel Z exchange, s -channel χ exchange, and the $ffH\eta$ contact interaction, as shown in Fig. 3. The amplitudes corresponding to these three diagrams are computed to be (from left to right)

$$i\mathcal{M}_I = \frac{\sqrt{2}}{vft_{2\beta}} \frac{-\xi m_Z^2}{q^2 - \xi m_Z^2} 2g_A m_f \bar{v}(p_{\bar{f}})\gamma^5 u(p_f), \quad (78)$$

$$i\mathcal{M}_{II} = \frac{\sqrt{2}}{vft_{2\beta}} \frac{q^2}{q^2 - \xi m_Z^2} 2g_A m_f \bar{v}(p_{\bar{f}})\gamma^5 u(p_f), \quad (79)$$

$$i\mathcal{M}_{III} = -\frac{\sqrt{2}}{vft_{2\beta}} 2g_A m_f \bar{v}(p_{\bar{f}})\gamma^5 u(p_f). \quad (80)$$

Here p_f and $p_{\bar{f}}$ are the four-momenta of f and \bar{f} , respectively and $q \equiv p_f + p_{\bar{f}}$. When we add the three contributions, we find

$$i\mathcal{M}_I + i\mathcal{M}_{II} + i\mathcal{M}_{III} = 0 \quad (81)$$

which is exactly what we would expect from field redefinition invariance. Moreover, we see that the Z and χ contributions add up to be gauge independent, while the contact interaction contribution itself is gauge independent.

Here we would like to mention a further subtle point related to the symmetric VSS vertex. It might still be somewhat counterintuitive that the contribution from the symmetric $ZH\eta$ vertex is canceled by the contribution from the $ffH\eta$ contact vertex, since the former contribution should know the position of the Z pole and therefore vanish for an on-shell Z boson, while the latter certainly does not “feel” the Z pole. To illustrate this issue, we can include the effect of the Z boson width Γ_Z so that the Z boson propagator in the unitarity gauge is written as

$$\frac{-g^{\mu\nu} + \frac{q^\mu q^\nu}{m_Z^2}}{q^2 - m_Z^2 + im_Z \Gamma_Z}. \quad (82)$$

When this propagator is dotted into q_ν coming from the symmetric VSS Feynman rule, at $q^2 = m_Z^2$ it will vanish, which seems quite plausible given our previous argument that a symmetric VSS vertex does not contribute to the process in which the related vector boson is on shell. However, this immediately leads to the paradoxical situation that near the on-shell region the field redefinition invariance is again violated since the contribution from the $ffH\eta$ contact vertex certainly does not know about the Z pole.

The resolution of this paradox consists in the treatment of the particle width in its propagator. The naive treatment in Eq. (82) is actually not quite correct and will in general lead to results that violate the Ward-Takahashi identities. A proper treatment can be made by, e.g., employing the complex mass scheme which properly retains gauge invariance. The final result is that, of course, no exotic structure appears near the Z pole and the field redefinition invariance is maintained.

IV. CONSTRAINTS FROM ELECTROWEAK PRECISION OBSERVABLES

As discussed in Sec. II, in the study of the pseudoaxion phenomenology there are eight sign combinations for the rotation parameters $\delta_t, \delta_{Dd}, \delta_{Ss}$. Moreover, when the lepton sector is relevant, either $t_\beta \geq 1$ or $t_\beta < 1$ could be possible, leading to further complications. Nevertheless, as will be shown in this section, the number of possibilities greatly reduces if we require the following.

- (1) The parameter space under consideration is favored by naturalness considerations and thus embodies (to some extent) the original motivation of the SLH model.
- (2) The parameter space under consideration is allowed by electroweak precision measurements.

As discussed in Sec. II, the first requirement points to the region characterized by a small top partner mass. In the SLH, currently the lower bound on the top partner mass is derived from Eq. (36) where f is stringently constrained by dilepton resonance searches. Constraints from direct searches for top partner production are not as competitive at the moment. For given f , a small top partner mass could be obtained by requiring a large t_β (or t_β^{-1} for $t_\beta < 1$), which is in turn bounded by unitarity considerations. To summarize, the first requirement points to the region characterized by a small f and large t_β (or t_β^{-1} for $t_\beta < 1$).

As for the second requirement, in the present work we consider the following electroweak observables.

- (1) The W boson mass m_W .
- (2) R observables measured at the Z pole, $R_b, R_c, R_e, R_\mu, R_\tau$, which are defined by

$$\begin{aligned} R_b &\equiv \Gamma(b\bar{b})/\Gamma(\text{had}), & R_c &\equiv \Gamma(c\bar{c})/\Gamma(\text{had}), \\ R_l &\equiv \Gamma(\text{had})/\Gamma(l^+l^-), & l &= e, \mu, \tau, \end{aligned} \quad (83)$$

in which $\Gamma(\text{had})$ denotes the total hadronic width of the Z boson, and $\Gamma(b\bar{b}), \Gamma(c\bar{c}), \Gamma(l^+l^-)$ denote the Z -boson partial widths into $b\bar{b}, c\bar{c}, l^+l^-$ channels. To set up the calculation we choose the fine-structure constant $\alpha_{\text{em}} \equiv \frac{e^2}{4\pi}$ (defined at the Z pole), the Fermi constant G_F , and Z boson mass m_Z as the input parameters. Expressed with the SM quantities, we have the tree-level relations

$$e = g_{\text{SM}} s_{W,\text{SM}}, \quad \frac{G_F}{\sqrt{2}} = \frac{g_{\text{SM}}^2}{8m_{W,\text{SM}}^2}, \quad (84)$$

$$m_Z^2 = \frac{g_{\text{SM}}^2 v_{\text{SM}}^2}{4c_{W,\text{SM}}^2}, \quad m_{W,\text{SM}}^2 = \frac{1}{4} g_{\text{SM}}^2 v_{\text{SM}}^2. \quad (85)$$

These relations are modified in the SLH to be

$$e = g_{SW}, \quad \frac{G_F}{\sqrt{2}} = \frac{g^2}{8m_{W,\text{SLH}}^2} \left(1 - \frac{v^2}{4f^2 t_\beta^2}\right)^2, \quad (86)$$

$$m_Z^2 = \frac{g^2 v^2}{4c_W^2} + \frac{g^2}{32c_W^2} \left[c_W^{-2}(3 - t_W^2) - \frac{4}{3} s_\beta^{-2} c_\beta^{-2} \right] \frac{v^4}{f^2}, \quad (87)$$

$$m_{W,\text{SLH}}^2 = \frac{1}{4} g^2 v^2 + \frac{1}{24} g^2 (3 - s_\beta^{-2} c_\beta^{-2}) \frac{v^4}{f^2}. \quad (88)$$

Here we note that in the above equations, as in Sec. II, g, v, s_W represent quantities in the SLH and are thus different from the SM quantities $g_{\text{SM}}, v_{\text{SM}}, s_{W,\text{SM}}$. From the above two sets of relations we may derive

$$\frac{m_{W,\text{SLH}}^2}{m_{W,\text{SM}}^2} = 1 + \frac{1}{8} \left(1 - t_{W,\text{SM}}^2 + \frac{1 - c_{W,\text{SM}}^2}{2c_{W,\text{SM}}^2 - 1} \frac{4}{t_\beta^2}\right) \frac{v_{\text{SM}}^2}{f^2}, \quad (89)$$

$$\frac{s_W^2}{s_{W,\text{SM}}^2} = 1 - \frac{1}{8} \left(1 - t_{W,\text{SM}}^2 + \frac{c_{W,\text{SM}}^2}{2c_{W,\text{SM}}^2 - 1} \frac{4}{t_\beta^2}\right) \frac{v_{\text{SM}}^2}{f^2}. \quad (90)$$

To calculate the R observables in the SLH we also need the modified Z couplings to light fermions. Although the corrections relative to the SM are of $\frac{v^2}{f^2}$ order, they are still relevant since the R observables have been measured to a few per mille precision. In such a case the diagonal entries in the rotational matrices in Eq. (49) should be understood as $1 - \frac{1}{2}\delta_{Dd}^2$ and $1 - \frac{1}{2}\delta_{Ss}^2$, respectively. Then the modified Z couplings to light fermions in the SLH can be written as

$$\begin{aligned}
g'_{L,Z,f} &= g_{L,Z,f} + \delta_Z g_{L,Z',f}, \\
g'_{R,Z,f} &= g_{R,Z,f} + \delta_Z g_{R,Z',f}, \\
&\text{for } f = u, c, b, e, \mu, \tau.
\end{aligned} \tag{91}$$

In the above equations, δ_Z is the $\mathcal{O}(\frac{v^2}{f^2})$ Z - Z' mixing angle, appearing in the mixing relation

$$Z' = Z'_m + \delta_Z Z_m, \quad Z = Z_m - \delta_Z Z'_m. \tag{92}$$

Here Z_m, Z'_m denote the final mass eigenstates after the $\mathcal{O}(\frac{v^2}{f^2})$ rotation while Z, Z' denote the states before the $\mathcal{O}(\frac{v^2}{f^2})$ rotation, as defined via Eq. (11). In the process of gauge boson mass diagonalization, δ_Z is computed to be

$$\delta_Z = -\frac{(1 - t_W^2)\sqrt{3 - t_W^2}v^2}{8c_W f^2}. \tag{93}$$

In Eq. (91), $g_{L,Z,f} = \frac{g}{c_W}(T_3^f - Q_f s_W^2)$, $g_{R,Z,f} = -\frac{g}{c_W}Q_f s_W^2$ are leading-order coefficients of the Lagrangian terms $\bar{f}_L \gamma^\mu f_L Z_\mu$, $\bar{f}_R \gamma^\mu f_R Z_\mu$, and T_3^f , Q_f denote the third components of the isospin and the electric charge of f , respectively. $g_{L,Z',f}$, $g_{R,Z',f}$ are leading-order coefficients of the Lagrangian terms $\bar{f}_L \gamma^\mu f_L Z'_\mu$, $\bar{f}_R \gamma^\mu f_R Z'_\mu$, which are given in Eqs. (64)–(66). $g'_{L,Z,f}$, $g'_{R,Z,f}$ in Eq. (91) denote the coefficients of the Lagrangian terms $\bar{f}_L \gamma^\mu f_L Z_\mu$, $\bar{f}_R \gamma^\mu f_R Z_\mu$ and T_3^f , Q_f , to $\mathcal{O}(\frac{v^2}{f^2})$ precision.

For $f = d$ the modified Z couplings in the SLH turn out to be

$$\begin{aligned}
g'_{L,Z,d} &= g_{L,Z,d} + \delta_Z g_{L,Z',d} + \delta_{Dd}^2 (g_{L,Z,D} - g_{L,Z,d}), \\
g'_{R,Z,d} &= g_{R,Z,d} + \delta_Z g_{R,Z',d}.
\end{aligned} \tag{94}$$

Obviously the additional correction is due to the left-handed D - d mixing. The corresponding formulas for $f = s$ can be obtained by the replacements $d \rightarrow s$, $D \rightarrow S$. $g_{L,Z,D}$, $g_{L,Z,S}$ are leading-order coefficients of the Lagrangian terms $\bar{D}_L \gamma^\mu D_L Z_\mu$, $\bar{S}_R \gamma^\mu S_R Z_\mu$,

$$g_{L,Z,D} = g_{L,Z,S} = \frac{1}{3} g s_W t_W. \tag{95}$$

Now we have all of the SLH couplings that are necessary to calculate the R observables. It should be noted that in the above coupling formulas, s_W , c_W , t_W are quantities in the SLH and are therefore different from their SM counterparts $s_{W,SM}$, $c_{W,SM}$, $t_{W,SM}$; see Eq. (90). Therefore, the modification of Z couplings to light fermions relative to the SM is caused by three factors: Z - Z' mixing, left-handed D - d , S - s mixing, and the correction of the weak-mixing angle.

A 95% C.L. constraint can be obtained in the f - t_β plane by performing a χ^2 fit of the five R observables. The χ^2 is defined by

TABLE I. Experimental values and the SM predictions of the R observables.

Quantity	Value	Standard Model
R_e	20.804 ± 0.050	20.737 ± 0.010
R_μ	20.785 ± 0.033	20.737 ± 0.010
R_τ	20.764 ± 0.045	20.782 ± 0.010
R_b	0.21629 ± 0.00066	0.21582 ± 0.00002
R_c	0.1721 ± 0.0030	0.17221 ± 0.00003

$$\chi^2 = \sum_{f=b,c,e,\mu,\tau} \frac{(R_{f,SLH} - R_f)^2}{\delta_{R_f}^2 + \delta_{R_{f,SM}}^2}. \tag{96}$$

In the above equation, R_f denotes the experimental values and δ_{R_f} denotes the associated experimental uncertainties. Also, $R_{f,SM}$ is the SM theory prediction and $\delta_{R_{f,SM}}$ denotes the associated theory uncertainty. Their values are listed in Table I [33]. As for the constraint from the W -boson mass, we treat it separately and consider two more precise measurements [33],

$$m_W = 80.387 \pm 0.016 \text{ GeV} \quad (\text{Tevatron}), \tag{97}$$

$$m_W = 80.370 \pm 0.019 \text{ GeV} \quad (\text{ATLAS}), \tag{98}$$

while we note that the SM prediction for m_W is [33]

$$m_{W,SM} = 80.358 \pm 0.004 \text{ GeV}. \tag{99}$$

In Fig. 4 the results of the electroweak precision analysis of m_W and R observables are shown. To clarify the situation we present the results according to whether $t_\beta \geq 1$ and the sign combination of the rotation parameters δ_{Dd} , δ_{Ss} [see Eq. (53)]. At first sight there are eight possibilities in total; however, it is immediately recognized that δ_{Dd}^+ , δ_{Ss}^- , and δ_{Dd}^- , δ_{Ss}^+ make no difference in terms of constraints in the f - t_β plane, reducing the number of possibilities to six. Therefore we obtain the six panels in Fig. 4, with each panel showing one possibility as described in the caption.

For all of the panels, the green and yellow regions correspond to parameter points that are allowed by the χ^2 fit of R observables at 68% and 95% C.L., respectively. These allowed regions do not exhibit a $t_\beta \rightarrow t_\beta^{-1}$ symmetry (e.g., the allowed regions in the upper right panel and the lower left panel still differ under the transformation $t_\beta \rightarrow t_\beta^{-1}$), since in the computation of R observables, the correction of s_W^2 relative to its SM value has to be taken into account, as was pointed out previously. When f is larger than about 17 TeV there will be a lower theoretical bound (from the mass relation) on t_β or t_β^{-1} which is larger than 1, corresponding to the white region at large f and small t_β or t_β^{-1} in each panel. The 2σ constraints from m_W measurements are simply implemented by requiring

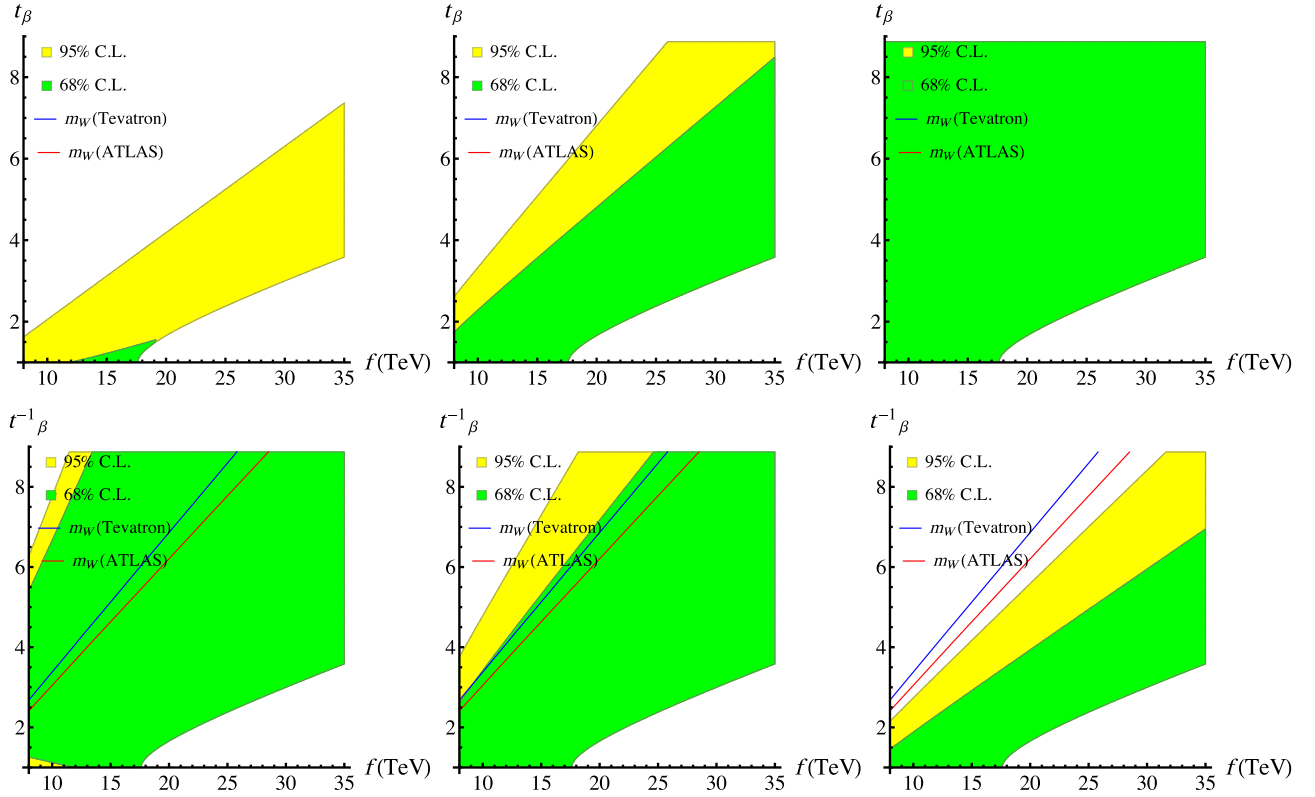


FIG. 4. Constraints from m_W and R observables in the f - t_β plane. Upper left: $t_\beta \geq 1$, δ_{Dd}^+ , δ_{Ss}^+ ; upper middle: $t_\beta \geq 1$, δ_{Dd}^+ , δ_{Ss}^- or $t_\beta \geq 1$, δ_{Dd}^- , δ_{Ss}^+ ; upper right: $t_\beta \geq 1$, δ_{Dd}^- , δ_{Ss}^- ; lower left: $t_\beta \leq 1$, δ_{Dd}^+ , δ_{Ss}^+ ; lower middle: $t_\beta \leq 1$, δ_{Dd}^+ , δ_{Ss}^- or $t_\beta \geq 1$, δ_{Dd}^- , δ_{Ss}^+ ; lower right: $t_\beta \leq 1$, δ_{Dd}^- , δ_{Ss}^- . See the text for a detailed description.

$$|m_{W,SLH} - m_W| < 2\sqrt{\delta_{m_W}^2 + \delta_{m_{W,SM}}^2}. \quad (100)$$

In the above equation m_W denotes the experimentally measured W -boson mass and δ_{m_W} and $\delta_{m_{W,SM}}$ denote the associated experimental and theoretical uncertainties, respectively. We superimpose the constraint boundary on the six plots as blue or red lines, representing constraints from Tevatron or ATLAS measurements, respectively. For all of these m_W constraint boundary lines, the regions on the right side of the lines are allowed at the 2σ level.

As can be seen from Fig. 4, if $t_\beta < 1$, then the region favored by naturalness consideration is disfavored by constraints from both R observables and W -boson mass measurements, regardless of the sign combination of the rotation parameters δ_{Dd} , δ_{Ss} . If $t_\beta \geq 1$, then W -boson mass measurements do not constrain the parameter region favored by naturalness consideration. However, in this case constraints from R observables are significant when any of the rotation parameters δ_{Dd} , δ_{Ss} adopt the plus sign in Eq. (53). This is because a plus sign leads to a large t_β enhancement of the rotation parameter and therefore a larger deviation of Z couplings to the corresponding fermion. Although the lower bound on f has been pushed to around 7.5 TeV by LHC dilepton resonance searches, the R observable constraints still force us to avoid this t_β

enhancement, and consequently the only possibility left is δ_{Dd}^- , δ_{Ss}^- with $t_\beta \geq 1$. This result has important consequences for the pseudoaxion phenomenology since the sign combinations of δ_{Dd} , δ_{Ss} will determine how η interacts with the D , S quarks which in turn influences the decay and production of the η particle, as will be discussed in more detail in the next section.

In previous literature on the SLH model the $t_\beta \geq 1$ and $t_\beta < 1$ cases are usually not distinguished, since a $t_\beta \rightarrow t_\beta^{-1}$ symmetry is tacitly assumed. Then only the $t_\beta \geq 1$ case is considered. However, strictly speaking this symmetry is only valid when the leptonic sector is not considered. Here we established clearly that if we consider the region favored by naturalness considerations, the $t_\beta < 1$ case is disfavored by measurements of m_W and R observables. This is closely related to the breakdown of the $t_\beta \rightarrow t_\beta^{-1}$ symmetry in the lepton sector. Moreover, in previous literature [12,24], the sign combination of the rotation parameter δ_{Dd} , δ_{Ss} was simply *assumed* to be (effectively) δ_{Dd}^- , δ_{Ss}^- , in order to suppress contributions to the electroweak precision observables. Here we also firmly establish this choice based on constraints from R observables, combined with m_W and naturalness considerations, keeping in mind that the constraint on f has been pushed to around 7.5 TeV due to updated LHC constraints.

V. PRODUCTION AND DECAY OF THE PSEUDOAXION

With the preparations made in the previous three sections, we are now ready to calculate the production and decay of the pseudoaxion. We will restrict ourselves to the region $2m_t \lesssim m_\eta \lesssim 1$ TeV, which is favored by naturalness considerations. All of the related partial width formulas are given in Appendix B.

A. Decay of the pseudoaxion

For η in the mass range $2m_t \lesssim m_\eta \lesssim 1$ TeV, it can always decay into $t\bar{t}$, gg , $\gamma\gamma$ channels. (The WW , ZZ , $Z\gamma$ channels are also possible and may have comparable branching ratios compared to $\gamma\gamma$. However, from a detection point of view, it is preferable to consider further decays into leptons in these channels, leading to an additional suppression by the leptonic branching. For simplicity we will not consider these channels further in this work.) $\eta \rightarrow ZH$ is highly suppressed, since the antisymmetric $ZH\eta$ vertex is suppressed to $\mathcal{O}(\frac{g^3}{f^3})$ while the symmetric $ZH\eta$ vertex does not contribute, as pointed out in Sec. III. If the new fermions D , S , N are heavy enough such that they cannot appear as decay products of η , then we are left with only the $t\bar{t}$, gg , $\gamma\gamma$ channels. Nevertheless, we should keep in mind that when f and m_η are given, the partial widths of these channels still depend on the masses of the additional heavy quarks T , D , S which do not appear as decay products of η . First, the $\eta \rightarrow t\bar{t}$ decay is controlled by the rotation parameter δ_t , which in turn depends on the top partner mass. The loop-induced decays $\eta \rightarrow gg$, $\gamma\gamma$ have contributions from both the top quark and the heavy quark partners T , D , S . The top quark contribution again depends on δ_t while the T , D , S contributions depend on the $\eta T\bar{T}$, $\eta D\bar{D}$, $\eta S\bar{S}$ couplings which are proportional to the corresponding rotation parameters times the quark partner mass. Experimentally, the current lower bound for the light-flavor quark partners D and S is around 700 GeV [34]. Thus, for a heavy enough η the $\eta \rightarrow Dd$, Ss channels are still possible

if the mass of D or S is close to the lower bound. To be definite, we will consider four benchmark scenarios.

- (1) Case A: $f = 8$ TeV, $m_T = m_D = m_S = 3$ TeV, all $m_N > m_\eta$.
- (2) Case B: $f = 8$ TeV, $m_\eta = 500$ GeV, $m_D = m_S = m_T$, all $m_N > m_\eta$.
- (3) Case C: $f = 8$ TeV, $m_T = 3$ TeV, $m_D = 700$ GeV, $m_S = 1$ TeV, all $m_N = 150$ GeV.
- (4) Case D: $f = 8$ TeV, $m_\eta = 500$ GeV, $m_D = m_S = m_T$, all $m_N = 150$ GeV.

For each case, there are two allowed sign combinations for the rotation parameters $(\delta_t, \delta_{Dd}, \delta_{Ss})$: $(+, -, -)$ and $(-, -, -)$. Other choices are excluded by electroweak precision measurements, if we are only interested in parameter regions favored by naturalness considerations. Therefore, in the following we will use Case A+, Case A-, etc., to indicate the sign choice of δ_t in each case [see Eq. (52)].

The total width and branching ratios of η are shown in Figs. 5 and 6 for Case A and Case B, respectively. In these two cases, the additional fermion partners D , S , N are not light enough to appear as decay products of η , and therefore we are left with the standard $\eta \rightarrow t\bar{t}$, gg , $\gamma\gamma$ channels. From the figures it is clear that η can be viewed as a narrow-width particle; however, the width is not small enough to give rise to displaced vertices. In both Case A and Case B and for both sign choices, η decays almost 100% to $t\bar{t}$, with only very small branching ratios to gg [$\mathcal{O}(0.1\%)$] and $\gamma\gamma$ [$\mathcal{O}(0.001\%)$]. Here (and in the following) all of the partial widths are calculated at LO, but it is obvious that the inclusion of higher-order radiative corrections has little effect on the whole picture. From a detection point of view, this situation is somewhat unfortunate since the dominant channel $t\bar{t}$ suffers from huge background at hadron colliders, while the clean channel $\gamma\gamma$ has an extremely small branching ratio. It is natural to ask how the situation will change if any of D , S , N is light enough, such that exotic channels like $\eta \rightarrow NN$, $N\nu$, Dd , Ss could be open. This is embodied in Cases C and D and we show the

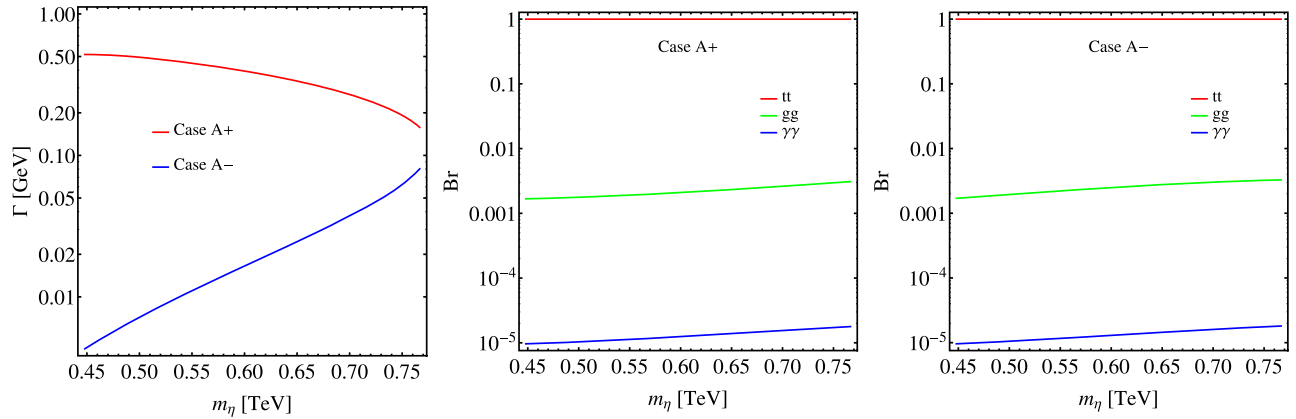
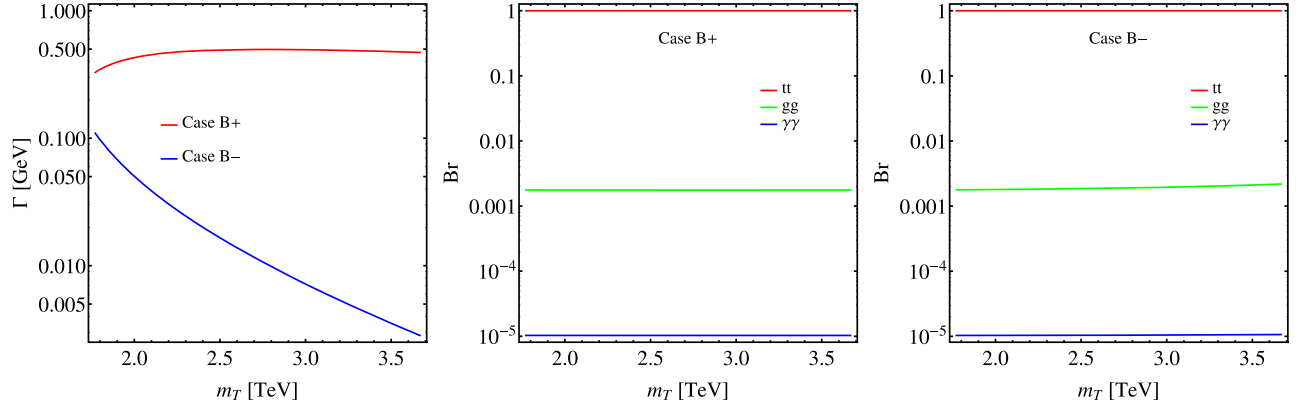


FIG. 5. Total width Γ and decay branching ratios of η in Case A.

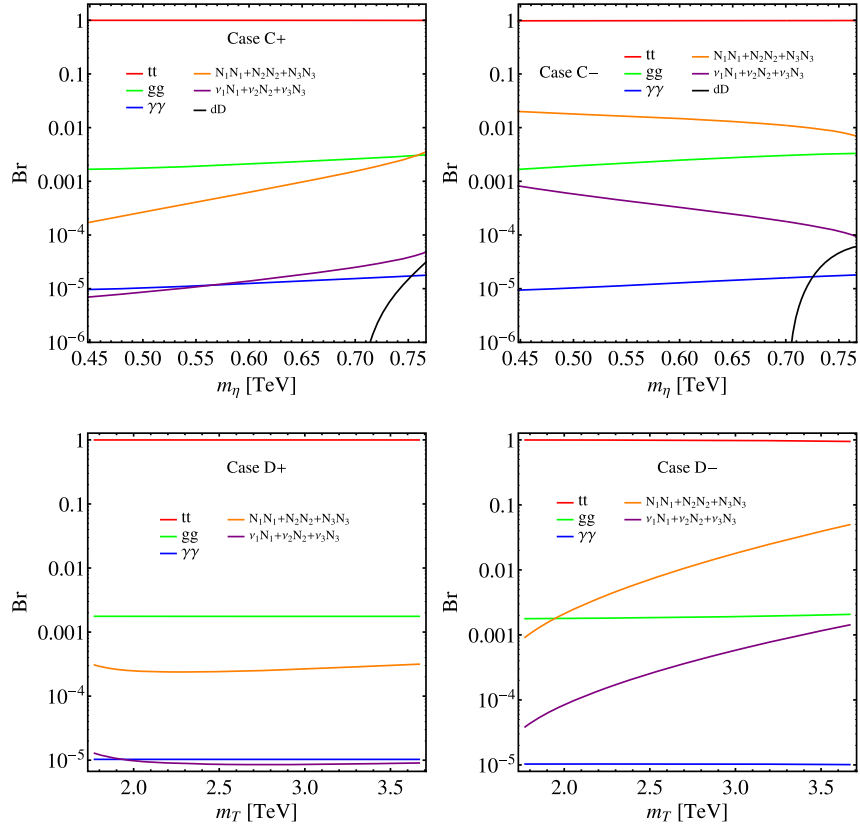
FIG. 6. Total width Γ and decay branching ratios of η in Case B.

corresponding branching ratio plots in Fig. 7. Nevertheless, the exotic channels contribute at most a few percent in terms of branching ratio, and therefore are of little use for η detection even if any of D , S , N is light enough. This can be understood from the interaction Lagrangian containing the ηDd , ηSs and $\eta N\nu$, ηNN vertices. The ηDd vertex is shown in Eq. (62). When $\eta \rightarrow Dd$ is open, $\frac{M_D}{v}$ is an $\mathcal{O}(1)$ quantity, and therefore from Eq. (62) we may recognize that the ηDd coupling can be considered as being relatively suppressed by $\mathcal{O}(\frac{v}{f})$ compared to the $\eta t\bar{t}$ vertex. This leads to the suppression of the $\eta \rightarrow Dd$ channel. The $\eta N\nu$ coupling is

relatively suppressed by $\mathcal{O}(\frac{v}{f})$ compared to the ηNN coupling, as can be seen from Eq. (60). However, when $\eta \rightarrow NN$ is open, M_{Nn} can be at most $\mathcal{O}(v)$. Moreover, the ηNN coupling suffers from a t_β suppression. Therefore, numerically the $\eta \rightarrow NN$ channel is much more suppressed compared to the $\eta \rightarrow t\bar{t}$ channel.

B. Decay of the top partner

The pseudoaxion may appear as a decay product of some additional heavy particles in the model. Among the additional particles in the SLH only Z' and T are closely related

FIG. 7. Decay branching ratios of η in Case C and Case D.

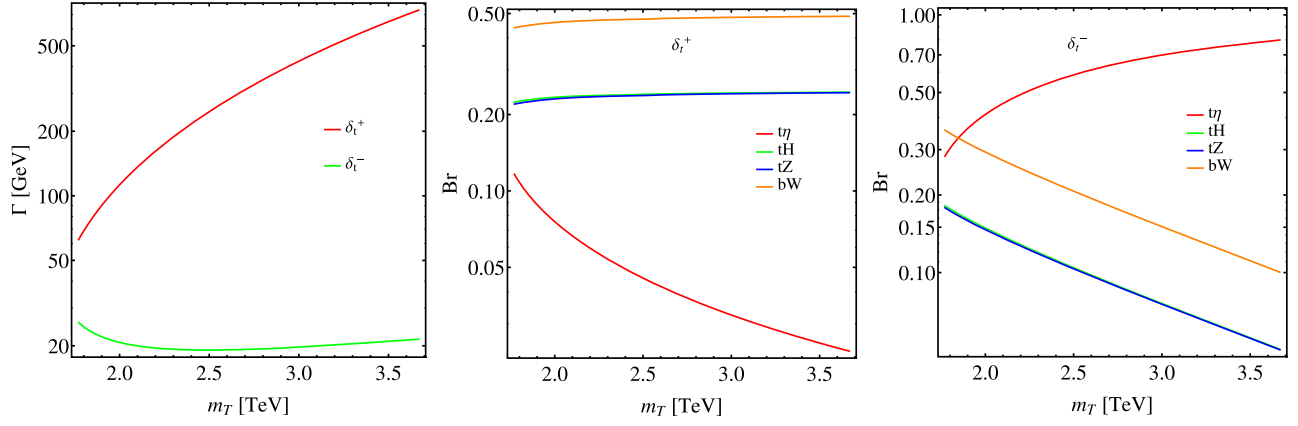


FIG. 8. Total width Γ and decay branching ratios of T in the SLH. We assume $f = 8$ TeV and $m_\eta = 500$ GeV. Note that in the considered mass range $T \rightarrow bX$, tY channels are not open.

to EWSB and naturalness favors small Z' and T masses within theoretical constraints. In this subsection we consider the decay of the top partner. The possibility of $T \rightarrow t + a$ (where T and a denote the top partner and a pNGB in the context of composite Higgs models) has been investigated in the literature [35–37]. Here we focus on the situation in the SLH. To be specific, we fix $f = 8$ TeV and $m_\eta = 500$ GeV and then plot the total width and branching ratios of T as functions of the top partner mass m_T in Fig. 8.

Both δ_i^+ and δ_i^- possibilities are considered. Note that when m_T is also given, according to the mass relation t_β can be calculated, which in turn determines the total width and branching ratios. The relation $\text{Br}(T \rightarrow bW) = 2\text{Br}(T \rightarrow tH) = 2\text{Br}(T \rightarrow tZ)$ holds to a good approximation. In the δ_i^+ case, $\text{Br}(T \rightarrow t\eta)$ is small (not larger than 10% for $m_T > 2$ TeV) and decreases with the increase of m_T . In the δ_i^- case, $\text{Br}(T \rightarrow t\eta)$ is sizable and becomes dominant (larger than 50%) for $m_T \gtrsim 2.2$ TeV. Another interesting

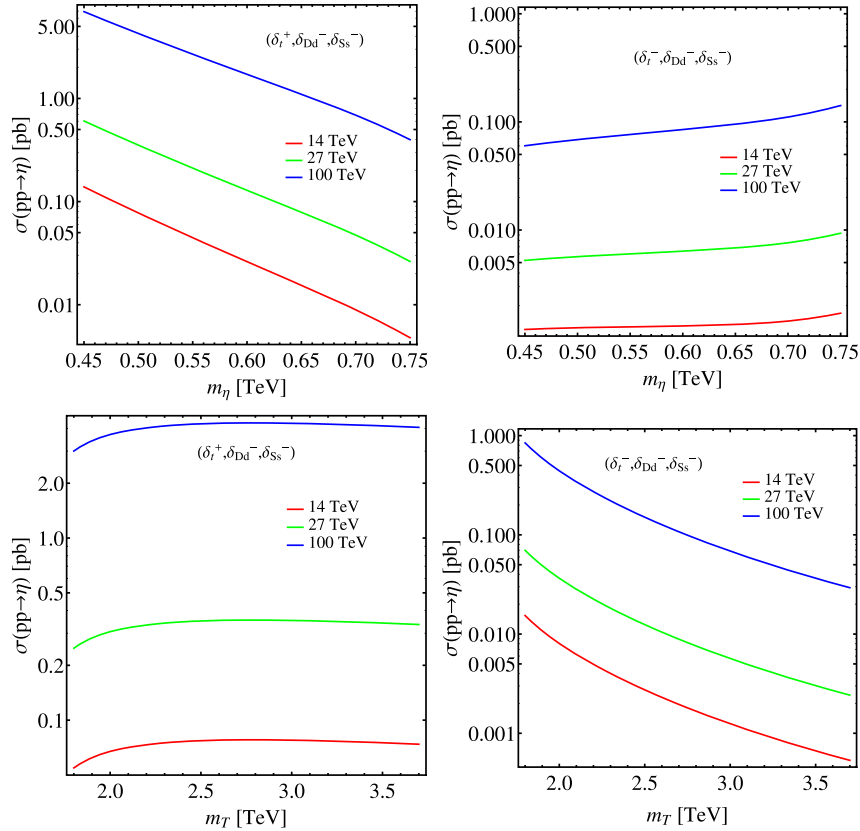


FIG. 9. Gluon-fusion production cross section of η as a function of m_η (upper panel, assuming $m_T = m_D = m_S = 3$ TeV) or m_T (lower panel, assuming $m_D = m_S = m_T$ and $m_\eta = 500$ GeV). The sign combination of $(\delta_i, \delta_{Dd}, \delta_{Ss})$ is indicated in each plot.

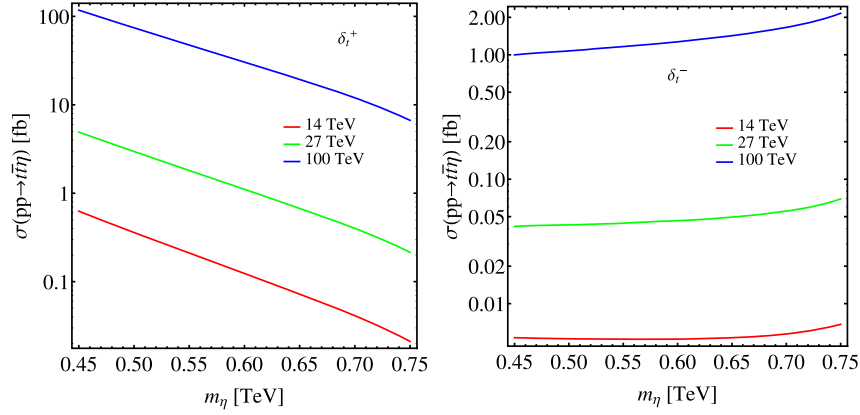


FIG. 10. Production cross section of $pp \rightarrow t\bar{t}\eta$ as a function of m_η . We assume $f = 8$ TeV and $m_T = 3$ TeV.

and important feature concerns the total width of T . In the δ_i^- case, the total width is around 20 GeV which makes the narrow-width approximation valid to high precision. In the δ_i^+ case, the total width increases with m_T . For $m_T \approx 3.5$ TeV the total width increases to around 500 GeV. In this case $\Gamma/M \lesssim 20\%$ and the narrow-width approximation still roughly holds, if the phase space is large enough. However, the width will have an appreciable impact on the invariant mass distribution of the T decay products.

C. Direct production of the pseudoaxion

The pseudoaxion can be directly produced via the gluon-fusion mechanism at hadron colliders. The particles running in the loop now contain t, T, D, S . In the calculation of the production cross section,¹⁰ we consider the 14 TeV (HL-)LHC, the 27 TeV HE-LHC, and the 100 TeV FCC-hh. The production cross sections are plotted in Fig. 9 as functions of m_η or m_T , with other parameters described in the figure caption. Although the production cross section may reach $\mathcal{O}(\text{pb})$ in certain regions of parameter space, unfortunately when combined with η decay it becomes very difficult to detect in the gluon-fusion channel. The dominant $t\bar{t}$ decay mode suffers from huge background, while the $\gamma\gamma$ decay mode has only a $\mathcal{O}(10^{-5})$ branching ratio.

Another way to directly produce η is through the $pp \rightarrow t\bar{t}\eta$ channel. We plot the production cross section as a function of m_η in Fig. 10, for three center-of-mass energies and both δ_i^+ and δ_i^- . Here we fix $f = 8$ TeV and $m_T = 3$ TeV, and therefore for a given m_η , t_β (and δ_i^\pm) is also determined. The cross section in the δ_i^- case is much

smaller than that in the δ_i^+ case. Even in the δ_i^+ case the detection of the $pp \rightarrow t\bar{t}\eta$ process is still very difficult. For instance, if we take $m_\eta = 450$ GeV, then in the δ_i^+ case the cross section reaches only about 0.6 fb at 14 TeV and 100 fb at 100 TeV. When we consider $\eta \rightarrow t\bar{t}$ decay, there exists the SM four-top production as an irreducible background, with a cross section of about 10 fb at 14 TeV and 5000 fb at 100 TeV. Unfortunately, since m_η is not far above the $2m_t$ threshold, we do not expect large differences in kinematical features between the $pp \rightarrow t\bar{t}\eta$ signal and the SM four-top background, making the discrimination very difficult. With larger m_η (say, 1 TeV), the top pair from η decay can be boosted, with an invariant mass distribution that peaks around a high value, which can facilitate the discrimination from SM backgrounds. However, the cross section for such a heavy η becomes very small. Therefore, we do not expect $pp \rightarrow t\bar{t}\eta$ to be a promising channel for future η detection in the SLH.

D. Pseudoaxion production from top partner decay

The above discussion shows that it is very difficult to detect η via the gluon-fusion and $t\bar{t}\eta$ -associated production channels. It is therefore natural to consider alternative η production mechanisms, such as decay from heavier particles. In the SLH, particles that can be heavier than η are T, D, S, N, Z', X and Y . Here we will concentrate on T , which is most tightly connected to EWSB. We will briefly comment on the possibility of detecting η from other heavy particle decays in the next subsection.

Under current constraints, the lower bound on m_T is already larger than the largest possible value of m_η plus m_t , and therefore the exotic decay channel $T \rightarrow t\eta$ will always be open. The branching fraction of $T \rightarrow t\eta$ has been discussed (see Fig. 8). Here we focus on top partner production. Two major production mechanisms are pair production through QCD interaction, and single production through the TbW vertex. Pair production has the virtue of being model independent, while single production depends on the value of δ_i . In Fig. 11 we present the cross sections of

¹⁰For simplicity, in this work all of the cross sections are calculated at LO using MADGRAPH5_AMC@NLO [38] and FEYNRULES [39]. We use the MSTW2008lo68cl parton distribution function [40]. For $2 \rightarrow 1$ production, the renormalization and factorization scale is taken to be the rest mass of the s -channel resonance. Otherwise, the renormalization and factorization scale is taken to be the sum of the transverse masses of final-state particles (before resonance decay) divided by 2.

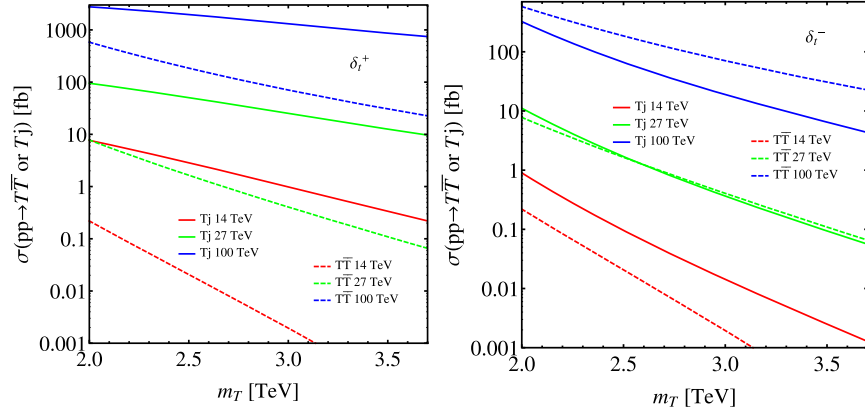


FIG. 11. Production cross sections of $pp \rightarrow T\bar{T}$ and $pp \rightarrow Tj$ as functions of m_T . We assume $f = 8$ TeV and $m_\eta = 500$ GeV. For $pp \rightarrow Tj$, the contribution from $pp \rightarrow \bar{T}j$ is also included.

$pp \rightarrow T\bar{T}$ and $pp \rightarrow Tj + \bar{T}j$ for both δ_i^+ and δ_i^- , as functions of m_T while we fix $f=8$ TeV, $m_\eta = 500$ GeV. Three center-of-mass energies (14, 27, 100 TeV) are considered. Whether pair or single production delivers a larger cross section depends on the sign choice for δ_i and the center-of-mass energy. In the δ_i^+ case, for all three center-of-mass energies the single production cross section is larger. In the δ_i^- case, at 14 TeV single production is

larger since pair production is highly suppressed by phase space. At 27 TeV pair production and single production become comparable, while for 100 TeV collider energy pair production dominates.

To detect η we would also like to consider the top partner decay $T \rightarrow t\eta$ that follows the pair or single production of T . The associated cross sections are plotted as functions of m_T in Fig. 12, using the narrow-width approximation, for

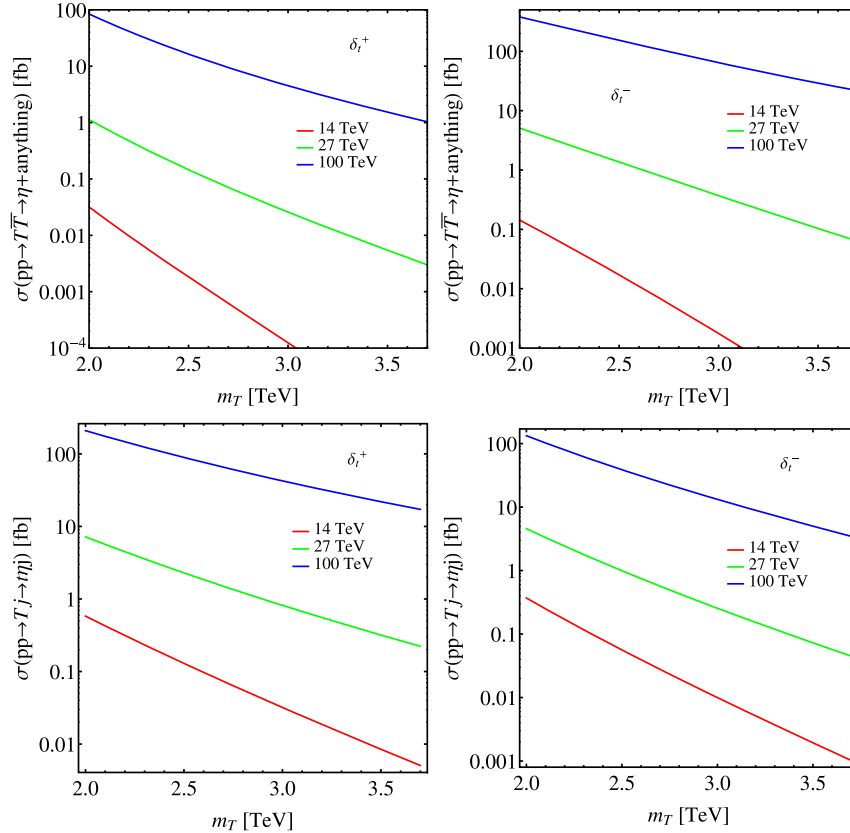


FIG. 12. Cross sections of $pp \rightarrow T\bar{T} \rightarrow \eta + \text{anything}$ and $pp \rightarrow Tj \rightarrow \eta + \text{anything}$ as functions of m_T . We assume $f = 8$ TeV and $m_\eta = 500$ GeV. For $pp \rightarrow Tj$, the contribution from $pp \rightarrow \bar{T}j$ is also included.

both δ_t^+ and δ_t^- . For definiteness we take $f = 8$ TeV, $m_\eta = 500$ GeV. To be precise, the plotted cross sections are defined by (for $pp \rightarrow Tj$, the contribution from $pp \rightarrow T\bar{j}$ is also included)

$$\sigma(pp \rightarrow Tj \rightarrow \eta + \text{anything}) = \sigma(pp \rightarrow Tj) \times \text{Br}(T \rightarrow t\eta), \quad (101)$$

$$\begin{aligned} \sigma(pp \rightarrow T\bar{T} \rightarrow \eta + \text{anything}) \\ = 2\sigma(pp \rightarrow T\bar{T}) \times \text{Br}(T \rightarrow t\eta)(1 - \text{Br}(T \rightarrow t\eta)) \\ + \sigma(pp \rightarrow T\bar{T}) \times \text{Br}^2(T \rightarrow t\eta). \end{aligned} \quad (102)$$

For the purpose of η detection, let us consider using the $\eta \rightarrow t\bar{t}$ channel, which has an almost 100% branching fraction. Then, the η production from top partner decays generically leads to a multitop (≥ 3) signature. Moreover, the top quarks will be boosted since $m_T \gg m_t + m_\eta$. For example, suppose a 2 TeV top partner is produced with little boost in the lab frame and then decays into $t + \eta$. At this step, t and η roughly share the rest energy of the top partner and therefore will each have about 1 TeV energy. The η boson then further decays into t and \bar{t} , each of which roughly has an energy of about 0.5 TeV. All three top quarks are boosted: the first one will have a decay ($t \rightarrow bW$) cone size approximated by $\sim 2m_t/E_t \simeq 0.4$, while the second and third top have $\sim 2m_t/E_t \simeq 0.8$. Furthermore, the second and third top quark decaying from η are close to each other, separated by approximated $\sim 2m_\eta/E_\eta \simeq 0.8$.

In the single production case, the signature will be $3t + j$, in which the first top is highly boosted while the second and third are still somewhat boosted and close to each other. One can make use of such kinematics to discriminate from QCD backgrounds. The most serious background is perhaps multitop production. One may be able to reduce the background using the *boosted* techniques [41]. In the pair production case, if we consider one top partner decaying into $t\eta$ with the other decaying into bW , we obtain a signature of $3t + b + W$ in which the top quarks and also the W boson will be boosted. In both the single and pair production channels, the invariant mass peaks at m_T and m_η will also be helpful in discriminating between the signal and background. Nevertheless, a full signal-background analysis using boosted-top techniques is beyond the scope of the present work.

From Fig. 12, we see that the cross sections at the 14 TeV (HL-)LHC for all of these channels are very small (< 1 fb), making the detection very difficult. Nevertheless, with the increase of collider energy, the signal cross sections increase significantly. For example, at the 100 TeV FCC-hh, for both δ_t^+ and δ_t^- and pair and single production channels, at relatively small m_T the cross sections could reach $\mathcal{O}(100)$ fb). In the δ_t^+ case, the single production (with the top partner decaying to $t\eta$) provides a cross

section of about 200 fb, which is larger than the pair production channel. In the δ_t^- case, the pair production (with one top partner decaying to $t\eta$) provides a cross section of about 400 fb, which is however larger than the single production channel.

In principle, top partner production and decay provide a way to measure t_β (which is important for testing the SLH mass relation) and also discriminate between the δ_t^+ and δ_t^- cases. In practice, we may consider the partial-width ratio $R_\eta \equiv \frac{\Gamma(T \rightarrow t\eta)}{\Gamma(T \rightarrow bW)}$ as both an indicator of the sign choice for δ_t and a way to measure δ_t , which in turn determines t_β . δ_t can also be determined from $pp \rightarrow Tj$ production since the cross section is proportional to δ_t^2 . Furthermore, in the δ_t^+ case the total width of T could reach $\mathcal{O}(100)$ GeV, which may have an impact on the invariant mass distribution of T decay products (e.g., bW). Measurement of the T total width in principle could also help determine the value of δ_t . However, even if δ_t is determined (including the sign choice), the determination of t_β and the test of the mass relation still require the measurement of f and m_η , which can be obtained if we are able to measure the masses of Z' and η particles.

E. Comments on other channels

Currently the SLH is stringently constrained by the LHC $Z' \rightarrow ll$ search; nevertheless, it also means that if the SLH was realized in nature, the $Z' \rightarrow ll$ signature would be the first place that we might expect the appearance of new physics. Then it would also be important to consider whether we may detect η as a decay product of Z' . Two channels might be considered: $Z' \rightarrow \eta H$ and $Z' \rightarrow \eta Y$. However, it turns out they give too small branching fractions: $\text{Br}(Z' \rightarrow \eta H) < 0.01$ and $\text{Br}(Z' \rightarrow \eta Y) < 10^{-4}$. This is regardless of whether the $Z' \rightarrow DD$, SS , NN channels are kinematically allowed. Therefore, it is not preferable to consider detecting η from Z' decay.

If kinematically allowed, we might also consider $D \rightarrow d\eta$, $S \rightarrow s\eta$, $N \rightarrow \nu\eta$ decays. However, these decay channels also suffer from small branching fractions, since the ηDd , ηSs , $\eta N\nu$ couplings are $\mathcal{O}(\frac{v}{f})$ suppressed compared to HDd , HSs , $HN\nu$ couplings [see Eqs. (60) and (62)]. For example, D will dominantly decay to uW , dZ , dH , with only $\text{Br}(D \rightarrow d\eta) < 1\%$, for the benchmark point $f = 8$ TeV, $m_T = 2$ TeV, $m_\eta = 0.5$ TeV and any value of m_D . Here δ_{Dd}^- is assumed, to be consistent with electroweak precision constraints. As for D production, for the δ_{Dd}^- case, there is a t_β^{-1} suppression for single D production, and therefore D pair production is more promising. Moreover, current collider constraints on the D mass are not stringent, such that $m_D = 700$ GeV is still allowed [34]. Therefore, if m_D is as light as 700 GeV, the large $pp \rightarrow D\bar{D}$ production cross section could compensate for the small $D \rightarrow d\eta$ branching fraction, leading to a sizable η production rate.

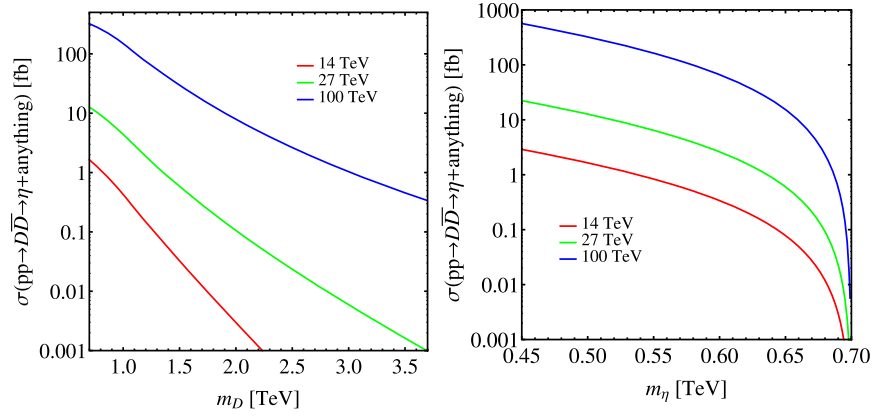


FIG. 13. Production cross section of $pp \rightarrow D\bar{D} \rightarrow \eta + \text{anything}$ as a function of m_D (left) and m_η (right). For the left plot, we assume $f = 8$ TeV, $m_T = 3$ TeV, $m_\eta = 500$ GeV. For the right plot, we assume $f = 8$ TeV, $m_T = 3$ TeV, $m_D = 700$ GeV.

At the 100 TeV FCC-hh, the η production cross section from D decay, $\sigma(pp \rightarrow D\bar{D} \rightarrow \eta + \text{anything})$ could also reach more than 100 fb for m_D not much larger than 700 GeV (see Fig. 13). This is comparable to the η cross section from top partner production, and in principle could also be used to measure t_β . The expected signature would be $t\bar{t} + 2j + W/Z/H$, in which the $W/Z/H$ should be boosted. The existence of various intermediate resonances would be helpful in discriminating signal and background. Nevertheless, we should be aware that naturalness does not offer any guidance on the preferred value of m_D . This is different from the case of m_T , in which naturalness clearly favors a lighter top partner. The case of $pp \rightarrow S\bar{S}$ production with $S \rightarrow s\eta$ decay is completely similar to the above discussion of D production and decay. For N , $\text{Br}(N \rightarrow \nu\eta)$ is also very small (less than 1% for the benchmark point $f = 8$ TeV, $m_T = 2$ TeV, $m_\eta = 0.5$ TeV and any value of m_N). Moreover, N does not have QCD pair production channels like D , S , and therefore it is difficult to detect η from N decay at hadron colliders.

The X , Y gauge bosons in the SLH may have decays like $X \rightarrow \eta W$ and $Y \rightarrow H\eta$. However, the single production cross sections of X , Y at hadron colliders are highly suppressed, and we need to rely on production with other heavy particles (heavy gauge bosons or quark partners) [24]. Since X , Y bosons are quite heavy (with masses of about $0.8m_{Z'}$), their production with other heavy particles would be limited by phase space while their decays are expected to be dominated by fermionic final states. Therefore, we do not consider η production from X , Y decays as promising channels for η detection.

VI. DISCUSSION AND CONCLUSIONS

The simplest little Higgs model provides a simple way to concretely realize the collective symmetry breaking mechanism, in order to alleviate the Higgs mass naturalness problem. In the scalar sector, its particle content is very economical, since besides the CP -even Higgs which should

serve as the 125 GeV Higgs-like particle, the only additional scalar particle is the pseudo-Nambu-Goldstone particle η associated with a remnant global $U(1)$ symmetry. The detection of η is important since its mass enters into the crucial SLH mass relation and it will also play an important role in discriminating SLH from other new physics scenarios. In this work we have been concerned with the production and decay of the η particle at future hadron colliders. We found that for natural regions of parameter space, m_η is larger than $2m_t$ and decays almost exclusively to $t\bar{t}$, and $\text{Br}(\eta \rightarrow \gamma\gamma)$ is too small to be considered promising for detection. Also, it is very difficult to detect η in the direct production channels $pp \rightarrow \eta$ (gluon fusion) and $pp \rightarrow t\bar{t}\eta$. Channels that are worth further consideration include η production from heavy quark partner (T , D , S) decays, in which the heavy quark partner might be singly (for T) or pair produced. The corresponding η production cross section at the 100 TeV FCC-hh could reach $\mathcal{O}(100 \text{ fb})$ for certain ranges of parameter space that are allowed by current constraints, while at the 14 TeV (HL-)LHC the rate might be too small for detection. However, the detection prospects in these channels (at 100 TeV) might still be challenging since the final states are quite complicated, including multijet-associated production with other objects, in which one or more of them could be boosted, requiring sophisticated tagging techniques. At the same time, the SM background also enjoys a large increase with the collider energy, with more a complicated hadronic environment. The aim of this paper was to examine the η production channels with a LO estimate of the η cross sections in the relatively promising ones as functions of the model parameters, keeping in mind the most up-to-date theoretical and experimental constraints (see Table II for a summary). We did not attempt to give a quantitative assessment of the collider sensitivities in these channels.

The phenomenology of the η particle in the SLH was studied a long time ago in several papers (e.g., Refs. [17,18,20,21]). Compared to all of the previous

TABLE II. Summary of η production from T , $D(S)$ decays at the 100 TeV FCC-hh. For $pp \rightarrow Tj$, the contribution from $pp \rightarrow \bar{T}j$ is also taken into account. For $T\bar{T}$, Tj channels, the benchmark point is $f = 8$ TeV, $m_T = 2$ TeV, $m_\eta = 500$ GeV while for $D\bar{D}$ channels, the benchmark point is $f = 8$ TeV, $m_T = 3$ TeV, $m_\eta = 500$ GeV, $m_D = 700$ GeV. When listing the signatures for $T\bar{T}$, $D\bar{D}$ channels we do not consider the situation in which both quark partners decay into $\eta + t$ or $\eta + j$, but this possibility is taken into account in the cross section values and plots.

Channel	Cross section at the benchmark point ($\sqrt{s} = 100$ TeV) (fb)	Signature
$pp \rightarrow T\bar{T} \rightarrow \eta + \text{anything}$	$84(\delta_t^+), 379(\delta_t^-)$	$3t + W + b$ or $4t + Z/H$
$pp \rightarrow Tj \rightarrow \eta + \text{anything}$	$209(\delta_t^+), 133(\delta_t^-)$	$3t + j$
$pp \rightarrow D\bar{D} \rightarrow \eta + \text{anything}$	322	$2t + W/Z/H + 2j$

studies, the present paper is different in a few crucial aspects.

- (1) Instead of working with the *ad hoc* assumption of no direct contribution to the scalar potential from the physics at the cutoff, we took into account in all calculations the crucial SLH mass relation (29) which is a reliable prediction of the SLH. Therefore, our prediction preserves all of the correlations required by theoretical consistency but does not depend on the choice of any fixed cutoff value such as $4\pi f$.
- (2) We have focused our attention on the parameter region favored by naturalness considerations. This region is characterized by small m_T and large t_β or t_β^{-1} . The favored η mass is larger than $2m_t$.
- (3) We have taken into account the recent collider constraint on f ($f \gtrsim 7.5$ TeV) which is much more stringent than the constraints obtained a long time ago. We also took into account the constraint from perturbative unitarity which sets an upper bound on the allowed value of t_β or t_β^{-1} . These two factors determine the current lower bound on m_T and crucially affect the largest cross section that can be achieved in all channels.
- (4) Our study is based on an appropriate treatment of the diagonalization of the vector-scalar system in the SLH, and especially the field redefinition related to η . This affects the derivation of $ZH\eta$ vertices and also η coupling to fermions, which were not treated properly in previous works until Ref. [22].
- (5) We also clarified the role played by the symmetric VSS vertices that appear in the Lagrangian and how they are compatible with the general principles, like field redefinition invariance and gauge independence.

From our study it turns out that the detection of η at the 14 TeV (HL-)LHC will be very difficult, and therefore a pp collider with higher energy and larger luminosity, such as the 27 TeV HE-LHC or even the 100 TeV FCC-hh or SppC, is motivated to capture the trace of such an elusive particle. Moreover, generally we would expect some other SLH signatures (e.g., $Z' \rightarrow ll$, $T \rightarrow bW$ or $D \rightarrow uW$) to show up earlier than η signatures since η signatures are usually very

complicated (with multiple top quarks) and suffer from small rates. It is nonetheless important to study η properties since they are crucial in testing the SLH mass relation and also provide a basis for model discrimination.

ACKNOWLEDGMENTS

We thank Yue-Lin Sming Tsai for helpful discussion. P. Y. T. was supported by the World Premier International Research Center Initiative (WPI), MEXT, Japan. This work was supported in part by the Natural Science Foundation of China (Grants No. 11635001 and No. 11875072), the China Postdoctoral Science Foundation (Grant No. 2017M610992), and the MoST of Taiwan under grant No. 105-2112-M-007-028-MY3 and No. 107-2112-M-007-029-MY3.

APPENDIX A: CONVENTION CONVERSION

References [23,24] contain detailed treatments of the anomaly-free SLH model. However, they used different conventions and it is useful to establish a conversion rule to relate formulas between the two conventions. Reference [23] used the following covariant derivative expression:

$$D_\mu = \partial_\mu - igA_\mu^a T^a + ig_x Q_x B_\mu^x, \quad g_x = \frac{gt_W}{\sqrt{1 - t_W^2/3}}. \quad (\text{A1})$$

On the other hand, Ref. [24] used

$$D_\mu = \partial_\mu + igA_\mu^a T^a + ig_x Q_x B_\mu^x, \quad g_x = \frac{gt_W}{\sqrt{1 - t_W^2/3}}. \quad (\text{A2})$$

Therefore, to convert between the two conventions, we need

$$g \leftrightarrow -g, \quad t_W \leftrightarrow -t_W \quad (\text{A3})$$

if we assume $g_x \leftrightarrow g_x$ and $A_\mu^a \leftrightarrow A_\mu^a$, $B_\mu^x \leftrightarrow B_\mu^x$, $T^a \leftrightarrow T^a$, $Q_x \leftrightarrow Q_x$. The transformations of s_W and c_W are still not determined. For convenience, we would like to identify the

first-order gauge boson mass eigenstates Z, Z', A in both conventions, namely,

$$Z \leftrightarrow Z, \quad Z' \leftrightarrow Z', \quad A \leftrightarrow A. \quad (\text{A4})$$

Then, by comparing the first-order gauge boson mixing formulas in the two papers we are led to the following conversion rule for s_W and c_W :

$$c_W \leftrightarrow c_W, \quad s_W \leftrightarrow -s_W. \quad (\text{A5})$$

Using these rules, it is straightforward to convert between the two conventions. (Our present work adopts the same convention as in Ref. [23].) Then, e.g., the Lagrangian coefficient of $Z'f\bar{f}$ couplings will acquire a minus sign during conversion since $g \leftrightarrow -g$. However, the expression for δ_Z [see Eq. (93)] remains the same since $c_W \leftrightarrow c_W$.

APPENDIX B: PARTIAL-WIDTH FORMULAS

Let us define

$$F(x, y) \equiv \sqrt{(1+x+y)(1-x-y)(1+x-y)(1-x+y)}. \quad (\text{B1})$$

In particular, we have

$$\Gamma_{\eta \rightarrow gg} = \frac{m_\eta^3 \alpha_s^2}{128\pi^3 v^2} |-\delta_t A_{\frac{1}{2}}(\tau_t) + \delta_t A_{\frac{1}{2}}(\tau_T) + \delta_{Dd} A_{\frac{1}{2}}(\tau_D) + \delta_{Ss} A_{\frac{1}{2}}(\tau_S)|^2, \quad (\text{B7})$$

$$\Gamma_{\eta \rightarrow \gamma\gamma} = \frac{m_\eta^3 \alpha_{em}^2}{2304\pi^3 v^2} |-4\delta_t A_{\frac{1}{2}}(\tau_t) + 4\delta_t A_{\frac{1}{2}}(\tau_T) + \delta_{Dd} A_{\frac{1}{2}}(\tau_D) + \delta_{Ss} A_{\frac{1}{2}}(\tau_S)|^2. \quad (\text{B8})$$

Here $\tau_f \equiv m_\eta^2/4m_f^2$ and for $f = T, D, S$ we have $\tau_f \ll 1$. The function $A_{\frac{1}{2}}(\tau) \equiv 2f(\tau)/\tau$, where

$$f(\tau) = \begin{cases} \arcsin^2 \sqrt{\tau} & (\tau \leq 1), \\ -\frac{1}{4} \left(\ln \frac{1+\sqrt{1-1/\tau}}{1-\sqrt{1-1/\tau}} - i\pi \right)^2 & (\tau > 1). \end{cases} \quad (\text{B9})$$

(2) T decay:

$$\Gamma_{T \rightarrow wb} = \frac{g^2 \delta_t^2 m_T^3}{64\pi m_W^2} \left(1 + \frac{m_W^2}{m_T^2} - \frac{2m_W^4}{m_T^4} \right) F\left(0, \frac{m_W}{m_T}\right) \simeq \frac{\delta_t^2 m_T^3}{16\pi v^2}, \quad (\text{B10})$$

$$\Gamma_{T \rightarrow Zt} = \frac{g^2 \delta_t^2 m_T^3}{128\pi c_W^2 m_Z^2} \left(1 + \frac{m_Z^2 - 2m_t^2}{m_T^2} + \frac{m_t^4 + m_t^2 m_Z^2 - 2m_Z^4}{m_T^4} \right) F\left(\frac{m_t}{m_T}, \frac{m_Z}{m_T}\right) \simeq \frac{\delta_t^2 m_T^3}{32\pi v^2}, \quad (\text{B11})$$

$$\Gamma_{T \rightarrow Ht} = \frac{m_T^3 \delta_t^2}{32\pi v^2} \left(1 + \frac{m_t^2 - m_H^2}{m_T^2} \right) F\left(\frac{m_t}{m_T}, \frac{m_H}{m_T}\right) \simeq \frac{\delta_t^2 m_T^3}{32\pi v^2}, \quad (\text{B12})$$

$$F(0, x) = 1 - x^2, \quad \text{for } |x| \leq 1. \quad (\text{B2})$$

The partial-width formulas related to η, T, D, S, N, Z' decays are listed as follows.

(1) η decay: Tree-level decay channels (to fermion final states):

$$\Gamma_{\eta \rightarrow i\bar{i}} = \frac{3m_\eta}{8\pi} \left(\frac{m_t \delta_t}{v} \right)^2 \sqrt{1 - \frac{4m_t^2}{m_\eta^2}}, \quad (\text{B3})$$

$$\Gamma_{\eta \rightarrow dD} = \frac{3m_\eta}{8\pi} \left(\frac{m_D}{v} \right)^2 \left(\delta_{Dd}^2 + \frac{v^2}{2f^2} \right)^2 \left(1 - \frac{m_D^2}{m_\eta^2} \right)^2, \quad (\text{B4})$$

$$\Gamma_{\eta \rightarrow N\bar{N}} = \frac{m_\eta m_N^2}{16\pi f^2 t_\beta^2} \sqrt{1 - \frac{4m_N^2}{m_\eta^2}}, \quad (\text{B5})$$

$$\Gamma_{\eta \rightarrow \nu N} = \frac{m_\eta}{8\pi} \left(\frac{vm_N}{2f^2 s_\beta^2} \right)^2 \left(1 - \frac{m_N^2}{m_\eta^2} \right)^2. \quad (\text{B6})$$

Here we adopt the notation $\Gamma_{\eta \rightarrow dD} \equiv \Gamma_{\eta \rightarrow d\bar{D}} + \Gamma_{\eta \rightarrow D\bar{d}}$ and $\Gamma_{\eta \rightarrow \nu N} \equiv \Gamma_{\eta \rightarrow \nu\bar{N}} + \Gamma_{\eta \rightarrow \bar{\nu}N}$.

Loop-induced decay channels:

$$\Gamma_{T \rightarrow \eta t} = \frac{m_T m_t^2}{32\pi v^2} \left(1 + \frac{m_t^2 - m_\eta^2}{m_T^2}\right) F\left(\frac{m_t}{m_T}, \frac{m_\eta}{m_T}\right) \simeq \frac{m_T m_t^2}{32\pi v^2} \left(1 - \frac{m_\eta^2}{m_T^2}\right)^2. \quad (\text{B13})$$

(3) D, S, N decays:

$$\Gamma_{D \rightarrow W u} = \frac{g^2 \delta_{Dd}^2 m_D^3}{64\pi m_W^2} \left(1 + \frac{m_W^2}{m_D^2} - \frac{2m_W^4}{m_D^4}\right) F\left(0, \frac{m_W}{m_D}\right) \simeq \frac{\delta_{Dd}^2 m_D^3}{16\pi v^2}, \quad (\text{B14})$$

$$\Gamma_{D \rightarrow Z d} = \frac{g^2 \delta_{Dd}^2 m_D^3}{128\pi c_W^2 m_Z^2} \left(1 + \frac{m_Z^2}{m_D^2} - \frac{2m_Z^4}{m_D^4}\right) F\left(0, \frac{m_Z}{m_D}\right) \simeq \frac{\delta_{Dd}^2 m_D^3}{32\pi v^2}, \quad (\text{B15})$$

$$\Gamma_{D \rightarrow H d} = \frac{m_D^3 \delta_{Dd}^2}{32\pi v^2} \left(1 - \frac{m_H^2}{m_D^2}\right) F\left(0, \frac{m_H}{m_D}\right) \simeq \frac{\delta_{Dd}^2 m_D^3}{32\pi v^2}, \quad (\text{B16})$$

$$\Gamma_{D \rightarrow \eta d} = \frac{m_D^3}{32\pi v^2} \left(\frac{v^2}{2f^2} + \delta_{Dd}^2\right)^2 \left(1 - \frac{m_\eta^2}{m_D^2}\right)^2 \ll \Gamma_{D \rightarrow W u, Z d, H d}. \quad (\text{B17})$$

The same formulas hold for S decay channels with the replacements $\delta_{Dd} \rightarrow \delta_{Ss}$, $m_D \rightarrow m_S$, $D \rightarrow S$, $d \rightarrow s$, $u \rightarrow c$. They also hold for N decay channels with the replacements $m_D \rightarrow m_N$, $D \rightarrow N$, $d \rightarrow \nu$, $u \rightarrow \ell$ and $\delta_{Dd} \rightarrow \delta_{Dd}^- = \frac{v}{\sqrt{2}f t_\beta}$.

(4) Z' decay:

For $Z' \rightarrow f \bar{f}$ decay modes, assuming the interaction Lagrangian $\mathcal{L} \supset \sum_f g(a_L^f \bar{f}_L \gamma^\mu f_L + a_R^f \bar{f}_R \gamma^\mu f_R) Z'_\mu$, the decay width is given by

$$\Gamma_{Z' \rightarrow f \bar{f}} = \frac{N_c g^2 m_{Z'}}{24\pi} \left((a_L^f)^2 + (a_R^f)^2 \right) \left(1 - \frac{m_f^2}{m_{Z'}^2}\right) + 6a_L^f a_R^f \frac{m_f^2}{m_{Z'}^2} \sqrt{1 - \frac{4m_f^2}{m_{Z'}^2}}. \quad (\text{B18})$$

$N_c = 1$ for leptons and $N_c = 3$ for quarks. For SM quarks, we can take $m_f = 0$ since $m_{Z'} \sim \mathcal{O}(f)$. a_L^f and a_R^f can be extracted from Eqs. (64)–(66). Thus, the $Z' \rightarrow f \bar{f}$ decay widths are

$$\Gamma_{Z' \rightarrow \ell^+ \ell^-} = \frac{g^2 m_{Z'} ((1 - t_W^2)^2 + 4t_W^4)}{96\pi(3 - t_W^2)}, \quad (\text{B19})$$

$$\Gamma_{Z' \rightarrow \nu \bar{\nu}} = \frac{g^2 m_{Z'} (1 - t_W^2)^2}{96\pi(3 - t_W^2)}, \quad (\text{B20})$$

$$\Gamma_{Z' \rightarrow u \bar{u}} = \Gamma_{Z' \rightarrow c \bar{c}} = \frac{g^2 m_{Z'}}{72\pi} \left(\frac{3 - t_W^2}{4} + \frac{4t_W^4}{3 - t_W^2} \right), \quad (\text{B21})$$

$$\Gamma_{Z' \rightarrow d \bar{d}} = \Gamma_{Z' \rightarrow s \bar{s}} = \frac{g^2 m_{Z'}}{72\pi} \left(\frac{3 - t_W^2}{4} + \frac{t_W^4}{3 - t_W^2} \right), \quad (\text{B22})$$

$$\Gamma_{Z' \rightarrow b \bar{b}} = \frac{g^2 m_{Z'}}{72\pi(3 - t_W^2)} \left(\frac{(3 + t_W^2)^2}{4} + t_W^4 \right), \quad (\text{B23})$$

$$\Gamma_{Z' \rightarrow t \bar{t}} = \frac{g^2 m_{Z'}}{72\pi(3 - t_W^2)} \left(\frac{(3 + t_W^2)^2}{4} + 4t_W^4 \right), \quad (\text{B24})$$

$$\Gamma_{Z' \rightarrow N \bar{N}} = \frac{g^2 m_{Z'}}{24\pi(3 - t_W^2)} \left(1 - \frac{m_N^2}{m_{Z'}^2}\right) \sqrt{1 - \frac{4m_N^2}{m_{Z'}^2}}, \quad (\text{B25})$$

$$\Gamma_{Z' \rightarrow D\bar{D}, S\bar{S}} = \frac{g^2 m_{Z'}}{72\pi(3-t_W^2)} \left[((3-t_W^2)^2 + t_W^4) \left(1 - \frac{m_{D,S}^2}{m_{Z'}^2} \right) - 6t_W^2(3-t_W^2) \frac{m_{D,S}^2}{m_{Z'}^2} \right] \sqrt{1 - \frac{4m_{D,S}^2}{m_{Z'}^2}}, \quad (\text{B26})$$

$$\Gamma_{Z' \rightarrow T\bar{T}} = \frac{g^2 m_{Z'}}{72\pi(3-t_W^2)} \left[((3-2t_W^2)^2 + 4t_W^4) \left(1 - \frac{m_T^2}{m_{Z'}^2} \right) - 12t_W^2(3-2t_W^2) \frac{m_T^2}{m_{Z'}^2} \right] \sqrt{1 - \frac{4m_T^2}{m_{Z'}^2}}. \quad (\text{B27})$$

Decay widths in bosonic channels:

$$\Gamma_{Z' \rightarrow W^+ W^-} = \frac{g^2 m_{Z'} (1-t_W^2)^2}{192\pi(3-t_W^2)} \left(1 - \frac{4m_W^2}{m_{Z'}^2} \right)^{\frac{3}{2}} \left(1 + \frac{20m_W^2}{m_{Z'}^2} + \frac{12m_W^4}{m_{Z'}^4} \right) \simeq \frac{g^2 m_{Z'} (1-t_W^2)^2}{192\pi(3-t_W^2)}, \quad (\text{B28})$$

$$\Gamma_{Z' \rightarrow ZH} = \frac{g^2 m_{Z'} (1-t_W^2)^2}{192\pi(3-t_W^2)} F\left(\frac{m_Z}{m_{Z'}}, \frac{m_H}{m_{Z'}}\right) \left[F^2\left(\frac{m_Z}{m_{Z'}}, \frac{m_H}{m_{Z'}}\right) + \frac{12m_Z^2}{m_{Z'}^2} \right] \simeq \frac{g^2 m_{Z'} (1-t_W^2)^2}{192\pi(3-t_W^2)}, \quad (\text{B29})$$

$$\Gamma_{Z' \rightarrow H\eta} = \frac{g^2 m_{Z'} (v/f)^2}{24\pi(3-t_W^2)t_{2\beta}^2} F^3\left(\frac{m_H}{m_{Z'}}, \frac{m_\eta}{m_{Z'}}\right), \quad (\text{B30})$$

$$\Gamma_{Z' \rightarrow Y\eta} = \frac{g^2 m_{Z'} (v/f)^2}{384\pi c_W^4} F\left(\frac{m_Y}{m_{Z'}}, \frac{m_\eta}{m_{Z'}}\right) \left(2 + \frac{(m_{Z'}^2 + m_Y^2 - m_\eta^2)}{4m_{Z'}^2 m_Y^2} \right). \quad (\text{B31})$$

-
- [1] G. Aad *et al.* (ATLAS Collaboration), *Phys. Lett. B* **716**, 1 (2012).
- [2] S. Chatrchyan *et al.* (CMS Collaboration), *Phys. Lett. B* **716**, 30 (2012).
- [3] A. N. Schellekens, *Rev. Mod. Phys.* **85**, 1491 (2013).
- [4] J. F. Donoghue, *Annu. Rev. Nucl. Part. Sci.* **66**, 1 (2016).
- [5] N. Arkani-Hamed, A. G. Cohen, and H. Georgi, *Phys. Lett. B* **513**, 232 (2001).
- [6] N. Arkani-Hamed, A. G. Cohen, T. Gregoire, and J. G. Wacker, *J. High Energy Phys.* **08** (2002) 020.
- [7] N. Arkani-Hamed, A. G. Cohen, E. Katz, A. E. Nelson, T. Gregoire, and J. G. Wacker, *J. High Energy Phys.* **08** (2002) 021.
- [8] N. Arkani-Hamed, A. G. Cohen, E. Katz, and A. E. Nelson, *J. High Energy Phys.* **07** (2002) 034.
- [9] M. Schmaltz and D. Tucker-Smith, *Annu. Rev. Nucl. Part. Sci.* **55**, 229 (2005).
- [10] M. Perelstein, *Prog. Part. Nucl. Phys.* **58**, 247 (2007).
- [11] D. Dercks, G. Moortgat-Pick, J. Reuter, and S. Y. Shim, *J. High Energy Phys.* **05** (2018) 049.
- [12] J. Reuter and M. Tonini, *J. High Energy Phys.* **02** (2013) 077.
- [13] J. Reuter, M. Tonini, and M. de Vries, *J. High Energy Phys.* **02** (2014) 053.
- [14] X.-F. Han, L. Wang, J. M. Yang, and J. Zhu, *Phys. Rev. D* **87**, 055004 (2013).
- [15] D. E. Kaplan and M. Schmaltz, *J. High Energy Phys.* **10** (2003) 039.
- [16] M. Schmaltz, *J. High Energy Phys.* **08** (2004) 056.
- [17] W. Kilian, D. Rainwater, and J. Reuter, *Phys. Rev. D* **71**, 015008 (2005).
- [18] W. Kilian, D. Rainwater, and J. Reuter, *Phys. Rev. D* **74**, 095003 (2006); **74**, 099905(E) (2006).
- [19] K. Cheung, S.-P. He, Y.-n. Mao, C. Zhang, and Y. Zhou, *Phys. Rev. D* **97**, 115001 (2018).
- [20] K. Cheung and J. Song, *Phys. Rev. D* **76**, 035007 (2007).
- [21] K. Cheung, J. Song, P. Tseng, and Q.-S. Yan, *Phys. Rev. D* **78**, 055015 (2008).
- [22] S.-P. He, Y.-n. Mao, C. Zhang, and S.-h. Zhu, *Phys. Rev. D* **97**, 075005 (2018).
- [23] F. del Aguila, J. I. Illana, and M. D. Jenkins, *J. High Energy Phys.* **03** (2011) 080.
- [24] T. Han, H. E. Logan, and L.-T. Wang, *J. High Energy Phys.* **01** (2006) 099.
- [25] O. C. W. Kong, *J. Korean Phys. Soc.* **45**, S404 (2004).
- [26] O. C. W. Kong, *Phys. Rev. D* **70**, 075021 (2004).
- [27] Y.-n. Mao, *Phys. Rev. D* **97**, 075031 (2018).
- [28] F. del Aguila, M. Masip, and J. L. Padilla, *Phys. Lett. B* **627**, 131 (2005).
- [29] M. Aaboud *et al.* (ATLAS Collaboration), *J. High Energy Phys.* **10** (2017) 182.
- [30] A. M. Sirunyan *et al.* (CMS Collaboration), *J. High Energy Phys.* **06** (2018) 120.
- [31] C. S. Kim, K. Y. Lee, and J. Park, *Phys. Rev. D* **85**, 117702 (2012).
- [32] S. Weinberg, *The Quantum Theory of Fields. Vol. 1: Foundations* (Cambridge University Press, Cambridge, England, 2005).

- [33] J. Erler and A. Freitas, <http://pdg.lbl.gov/2018/reviews/rpp2018-rev-standard-model.pdf>.
- [34] A. M. Sirunyan *et al.* (CMS Collaboration), *Phys. Rev. D* **97**, 072008 (2018).
- [35] N. Bizot, G. Cacciapaglia, and T. Flacke, *J. High Energy Phys.* **06** (2018) 065.
- [36] J. Serra, *J. High Energy Phys.* **09** (2015) 176.
- [37] J. Kearney, A. Pierce, and J. Thaler, *J. High Energy Phys.* **10** (2013) 230.
- [38] J. Alwall, R. Frederix, S. Frixione, V. Hirschi, F. Maltoni, O. Mattelaer, H.-S. Shao, T. Stelzer, P. Torrielli, and M. Zaro, *J. High Energy Phys.* **07** (2014) 079.
- [39] A. Alloul, N. D. Christensen, C. Degrande, C. Duhr, and B. Fuks, *Comput. Phys. Commun.* **185**, 2250 (2014).
- [40] A. D. Martin, W. J. Stirling, R. S. Thorne, and G. Watt, *Eur. Phys. J. C* **63**, 189 (2009).
- [41] D. E. Kaplan, K. Rehermann, M. D. Schwartz, and B. Tweedie, *Phys. Rev. Lett.* **101**, 142001 (2008).